Diego Blaese

PROCESSING AND CHARACTERIZATION OF MONOCLINIC-ZIRCONIA FIBRE-MATRIX INTERFACES IN DENSE MATRIX ALUMINA-ALUMINA COMPOSITES

Dissertação submetida ao Programa de Pós-Graduação em Engenharia Mecânica da Universidade Federal de Santa Catarina para a obtenção do Grau de Mestre em Engenharia Mecânica
Orientador: Prof. Dr.-Ing. Márcio Celso Fredel

Florianópolis
2013

Blaese, Diego
Processing and characterization of monoclinic-zirconia fibre-matrix interfaces in dense matrix alumina-alumina composites / Diego Blaese ; orientador, Márcio Celso Fredel ; co-orientador, Dachamir Hotza. - Florianópolis, SC, 2013.
91 p.

Dissertação (mestrado) - Universidade Federal de Santa Catarina, Centro Tecnológico. Programa de Pós-Graduação em Engenharia Mecânica.

Inclui referências

1. Engenharia Mecânica. 2. fibre-matrix interfaces. 3. monoclinic zirconia. 4. ceramic matrix composites. 5. toughening mechanisms. I. Fredel, Márcio Celso . II. Hotza, Dachamir. III. Universidade Federal de Santa Catarina. Programa de Pós-Graduação em Engenharia Mecânica. IV. Título.

Diego Blaese

PROCESSAMENTO E CARACTERIZAÇÃO DE INTERFACES FIBRA-MATRIZ DE ZIRCÔNIA NÃO ESTABILIZADA EM COMPÓSITOS ALUMINA-ALUMINA DE MATRIZ DENSA

Esta Dissertação foi julgada adequada para obtenção do Título de Mestre em Engenharia Mecânica, e aprovada em sua forma final pelo Programa de Pós-graduação em Engenharia Mecânica.

Florianópolis, 28 de março de 2013.

_____
Prof. Márcio Celso Fredel, Dr.-Ing.
Orientador

_____
Prof. Dachamir Hotza, Dr.-Ing.
Coorientador

_____
Prof. Júlio César Passos, Dr.
Coordenador do Curso

Banca Examinadora:

_____
Prof. Márcio Celso Fredel, Dr.-Ing.
Presidente

_____
Prof. Hazim Ali Al-Qureshi, Ph.D.

_____
Prof. Édison da Rosa, Dr.Eng.

_____
Prof. Rolf Bertrand Schroeter, Dr.Eng.

“The absence of evidence is not the evidence of absence.”
Carl Sagan, *Cosmos*

ACKNOWLEDGEMENTS

I would like to thank:

Federal University of Santa Catarina together with my advisor Prof Dr.-Ing. Márcio Celso Fredel for this great opportunity;

Hamburg University of Technology (TUHH) and especially Prof. Dr.-Ing.Gerold Schneider and Dr.-Ing. Rolf Janssen from the Institute of Advanced Ceramics for supporting my internship;

Graduate Program in Mechanical Engineering (POSMEC) and Capes for the Brazilian scholarship;

My co-advidsor Prof Dr.-Ing. Dachamir Hotza and the Brazilian-German Collaborative Research Initiative on Manufacturing Technology (BRAGECRIM/CAPES) for the scholarship in Germany;

Dr.-Ing. Daniel Enrique Garcia for the supervision and great exchange of knowledge;

The institute colleagues, especially Paula Guglielmi for the great help and support towards the success of my work.

All my friends for the happy moment.

My dear Francielle Ana Grando for the love and kindness.

My family, Erwin H. Blaese, Marize H. Blaese and Susan Blaese for the love and encouragement.

Thank you!

ABSTRACT

Fibre-matrix interface properties play an important role on the performance of ceramic matrix composites. Being the fibre-matrix interaction too strong, the composite will behave such as a monolithic ceramic and being too weak, the composite will lose its structural integrity and its interlaminar properties. Monoclinic (unstabilized) zirconia has shown to be a suitable alternative for the production of fibre-matrix interfaces for alumina ceramic matrix composites due to its low chemical interaction during sintering and due to the microcracking phenomenon caused by the tetragonal-monoclinic transformation during cooling. Porous oxide coatings of monoclinic zirconia, which have low toughness because of their porosity and microcracking, have been used in the past to achieve debonding between sapphire fibres and alumina matrices and were to be chemically stable with sapphire above 1300 °C. Tough alumina matrix composites have been fabricated using monoclinic zirconia as fibres coating. However the matrix porosity was $\geq 13\%$, which makes it difficult to interpret the results, because the toughness cannot be unambiguously attributed to the properties of the unstabilized zirconia interfaces. In this work, model composites with dense alumina matrix and single alumina fibres were fabricated. The fibre-matrix interface was produced via dip-coating single fibres in monoclinic zirconia suspensions. Different particle sizes were used for the dip-coating in order to vary the coating porosity. The interfacial sliding stress was determined via a modified fibre pushin test. The crack deflection behaviour was analysed from cracks created via Vickers indentations and the fibre pullout via surface fracture observations. Properties such as fracture toughness, hardness and elastic modulus for the interface and matrix were also evaluated in order to determine the crack deflection parameters established by He and Hutchinson.

Keywords: fibre-matrix interfaces, ceramic matrix composites, monoclinic zirconia, crack deflection, fibre pullout, dip-coating.

RESUMO

Interfaces fibra-matriz tem um papel muito importante no desempenho de compósitos de matriz cerâmica. Sendo a interação entre fibra e matriz for muito forte, o compósito se comportará como uma cerâmica monolítica, e sendo muito fraca, o compósito perderá sua integridade estrutural e suas propriedades interlaminares. Zircônia monoclínica (não-estabilizada) tem mostrado ser uma boa alternativa na produção de interfaces fibra-matriz para compósitos cerâmicos à base de alumina devido à sua baixa interação química durante a sinterização e também devido ao fenômeno de microtrincamento causado pela transformação tetragonal-monoclínica durante o resfriamento. Interfaces porosas à base de zircônia monoclínica, as quais apresentam baixa tenacidade devido à sua porosidade e microtrincamento, haviam sido usadas no passado para criar interfaces com baixa interação entre fibras de safira e matrizes de alumina. Neste sistema, as interfaces se mostraram quimicamente estáveis mesmo acima de 1300 °C. Compósitos tenazes à base de alumina haviam sido fabricados com zircônia monoclínica como interface. Entretanto, a porosidade da matriz era $\geq 13\%$, o que dificulta a interpretação dos resultados, pois as propriedades mecânicas do compósito não podem ser claramente atribuídas às propriedades da zircônia monoclínica. Neste trabalho, compósitos-modelo com matriz densa e fibras individuais de alumina foram produzidos. A interface fibra-matriz foi produzida através de recobrimento por *dip-coating* das fibras em suspensões cerâmicas de zircônia monoclínica. Diferentes tamanhos de partícula foram utilizados no processo de *dip-coating* com o objetivo de variar a porosidade e assim, as propriedades das interfaces. A tensão de cisalhamento interfacial foi determinada através do teste de *pushin* nas fibras. O fenômeno de deflexão de trincas foi avaliado através de trincas criadas por indentação Vickers e o fenômeno de *pullout* das fibras através de observações nas superfícies de fratura. Propriedades como tenacidade à fratura, dureza e módulo de elasticidade da matriz e interface foram avaliadas para determinar os parâmetros de deflexão de trincas propostos por He e Hutchinson.

Palavras-chaves: interfaces fibra-matriz, compósitos de matriz cerâmica, zircônia não-estabilizada, *dip-coating*, deflexão de trincas, *pullout*.

LIST OF FIGURES

LIST OF TABLES

LIST OF ACRONYMSAND ABBREVIATIONS

Al_2O_3	aluminium oxide (alumina)
C	Carbon
$CaAl_{12}O_{19}$	hexa-aluminate hibonite
CMC	ceramic matrix composite
CVD	chemical vapor deposition
$LaPO_4$	monazite system
m-ZrO_2	monoclinic zirconia
NC	no coating (absence)
SEM	scanning electron microscope
SENB	single edge notched beam
SEVNB	single edge v-notched beam
Si_3N_4	silicon nitride
SiC	silicon carbide
SiO_2	silicon oxide (silica)
XRD	x-ray difraction
YPO_4	monazite system
Z015	0.15 μm particle size m-ZrO_2 coating
Z080	0.80 μm particle size m-ZrO_2 coating
ZrO_2	zirconium oxide (zirconia)

LIST OF SYMBOLS

Latin alphabet

A	linear regression parameter	
B	specimen witdh	[m]
E	elastic modulus	[Pa]
E_f	elastic modulus of the fibre	[Pa]
E_{ind}	elastic modulus of the indenter	[Pa]
E_m	elastic modulus of the matrix	[Pa]
E_m	elastic modulus of the material	[Pa]
F_M	maximum loading force	[N]
G_d	energy release rate for crack deflection	[J/m²]
G_f	fibre toughness	[J/m²]
G_i	interface toughness	[J/m²]
G_p	energy release rate for crack penetration	[J/m²]
h	coating thickness	[m]
h_f	final displacement	[m]
h_i	initial displacement	[m]
K_{IC}	fracture toughness	[Pa.m$^{1/2}$]
m	exponential regression parameter	
P	indentation load	[N]
R	fibre radius	[m]
S	stiffness during unloading	[N/m]
S_1	inner span in four-point bending	[m]
S_2	outer span in four-point bending	[m]
v	withdrawal speed	[m/s]
W	specimen height	[m]
Y*	intensity factor	

Greek alphabet

η	liquid viscosity	[N.s/m²]
Δ_*	reference displacement	[m]
Δ_n	loop width for a given cycle	[m]
Γ	toughness	[J/m²]
γ	gravitational acceleration	[m/s²]

γ_{LV}	liquid-vapor surface tension	[N/m]
ν_{ind}	Poisson`s ratio of the indenter	
ν_{m}	Poisson`s ratio of the material	
ρ	liquid density	[g/cm^3]
τ	interfacial sliding stress	[Pa]
α	elastic mismatch	
Σ	tendency for crack deflection to occur	

TABLE OF CONTENTS

1. INTRODUCTION

The present work is a result of a partnership program between Brazil and Germany, so called, Brazilian-German Collaborative Research Initiative on Manufacturing Technology (BRAGECRIM). The work was initiated at the Ceramic & Composite Materials Research Laboratories (CERMAT), UFSC, Brazil and by means of a Sandwich Master scholarship, was carried out at the Institute of Advanced Ceramics, TUHH, Germany.

Toughening mechanisms are needed to increase damage tolerance of ceramics. One of the most common techniques is the addition of reinforcements (often in the form of fibres) in the ceramic matrix, producing the so-called ceramic matrix composites (CMCs). Reinforcements promote mechanisms such as crack deflection, crack bridging and pullout that consume energy during fracture. For these mechanisms to be effective, the adhesion between the reinforcement (fibre) and the matrix, should be weak, otherwise, the material will behave like a monolithic ceramic.[1; 2]

The characteristics of the fibre-matrix interface play a decisive role in the performance of CMCs. If the interaction between fibre and matrix is too strong, the composite behaves as a monolithic ceramic, if the interaction is too weak, the composite will lose its structural integrity and its interlaminar properties.[2; 3] Thus, there is a need of studying and developing interfaces in CMCs, especially for those with dense, which are not so understood.[4]

An interface material needs to follow some fundamental requirements before being tested in CMCs. First, it should not degrade the fibre properties at any scale, because the fibres are responsible for carrying most of the load, therefore, no chemical reaction between fibre and interface can occur. Second, the interface must withstand high temperatures and corrosive environments without degradation. Third, the interface must be weak enough to promote toughening mechanisms such as crack deflection, crack bridging and fibre pullout, preventing premature failure of the fibres.

Monoclinic zirconia is shown as a good alternative for the production of oxide fibre-matrix interfaces in CMCs based on alumina, due to the absence of chemical interaction during sintering. Monoclinic zirconia undergoes a tetragonal-monoclinic phase transformation (1170 °C) during cooling and this transformation is accompanied by an increase in volume of

4%,[5] leading to the phenomenon of microcracking. Microcracking can reduce the fracture toughness of the fibre-matrix interface, yielding low fracture energy, which is main requirement for toughening of CMCs.

The application of this interface at high temperatures would also reduce the bonding between fibre and interface, i.e., the interfacial sliding stress, due to the decrease in volume during the monoclinic-tetragonal phase transformation.

2. AIM OF THE WORK

2.1. GENERAL AIM

The aim of this work is to develop fibre-matrix interfaces for oxide CMCs with long fibres and dense matrix, both of alumina. The proposal is to produce model composites with monoclinic zirconia-coated alumina fibres creating an interface sufficiently weak to promote toughening mechanisms.

2.2. SPECIFIC AIM

In order to achieve the overall goal the following specific objectives are aimed:

- Produce fibre-matrix interfaces by coating fibres via dip-coating using slurries of monoclinic (unstabilized) zirconia;
- Evaluate the influence of particle sizes on porosity, elastic modulus and fracture toughness of the interfaces in order to verify the condition of crack deflection as proposed by He and Hutchinson;
- Analyse the crack deflection toughening mechanism via Vickers indentation induced cracks;
- Determine the interfacial sliding stress of the fibre-matrix interfaces.
- Verify the fibre pullout toughening mechanism;
- Characterize the morphology of the fibre-matrix interfaces.

3. LITERATURE REVIEW

3.1. CERAMIC MATRIX COMPOSITES (CMCs)

Ceramic matrix composites (CMCs) are refractory materials designed to be applied in severe environments. These severe environments combine, in many cases, mechanical stresses and corrosive atmospheres. Compared to other materials such as steel, aluminium, titanium alloys, superalloys of nickel and monolithic ceramics, they are relatively new and are now well established in high technology applications. CMCs are characterized by having ceramic fibres in a ceramic matrix also with a relatively weak interaction between fibre and matrix. These weak interfaces differentiate CMCs from other materials, often having superior properties. The deformation of fracture of such materials is an order of magnitude higher than monolithic ceramics and the density is usually low, which results in good specific properties, being able overcome any other materials at temperatures above 1000 °C. These materials generally have long term stability and high creep resistance.[1; 2; 6]

3.1.1. Oxide CMCs

Chemical stability at high temperature in oxidizing and corrosive environments can be achieved when all constituents of the CMC are oxides: fibre, matrix and interface between fibre and matrix. The main ceramic materials used in CMCs are alumina (Al_2O_3), mullite ($3Al_20_3$-$2SiO_2$), zirconia (ZrO_2), among others. Moreover, adding fibres to some oxide composites can lead to reduction of costs more than, for example, in SiC-based composites. Superior resistance to severe environments of the oxide CMCs is given usually at the cost of loss of mechanical properties when compared with the non-oxide ceramic composites. One major problem presented in oxide CMCs is a relative low creep resistance due to the polycrystalline structure of the fibres. Oxide CMCs also have high thermal expansion coefficients and low thermal conductivity when compared to non-oxide composites. The design and development of components subjected to thermal shock has a high degree of complexity.[1; 2; 6]

3.1.2. Non-oxide CMCs

Non-oxide CMCs often exhibit high mechanical strength and creep resistance when compared to oxide CMCs. On the other hand, they show high susceptibility to oxidation at high temperature in oxidizing atmosphere, which leads to degradation of the structure over time; therefore, coating processes are needed for the reduction of the susceptibility to oxidation. The main constituent of non-oxide CMCs are silicon carbide (SiC), carbon (C) and silicon nitride (Si_3N_4).[2]

3.1.3. Applications

The demand for space technology played a decisive role in the development of CMCs. Structures for operation at high temperature, e.g., thermal protection systems, nozzle cones and rocket nozzles were developed for military and aerospace applications. Recently, CMCs began to be developed for civilian applications. Due to its high thermal stability and good resistance to corrosion and wear, these materials are having their range of applications expanded for other industries, such as transport systems in the form of clutches and brakes, mechanical construction, such as bearings and ballistic protections and energy generation in the form of burners, heat exchangers and pumps.[1; 2]

3.2. FIBRE-MATRIX INTERFACES

The interface between fibre and matrix is an important constituent in ceramic matrix composites. Depending on the characteristics of the interface, the CMC can either behave like a brittle material or as a damage tolerant composite.[1; 2] The basic requirement for having damage tolerant CMCs is that the cracks initiated in the matrix do not propagate through the fibres, but deflect along the interface, thus leaving the fibres intact as the crack advances. This phenomenon requires that the fibre/matrix interface or a region near the fibre is sufficiently weak to fail before the fibre fails.[6] Furthermore, the fibre-matrix interface is responsible for the crack bridging and fibre pullout toughening mechanisms which occur simultaneously with the deflection of cracks.

There are two basic approaches used to design damage tolerant CMCs. One utilizes a weak interface, which typically involves coating of the fibres and the other that involves the production of a porous matrix.[6; 7; 8; 9; 10] The porous matrix approach has been studied extensively, therefore, greater efforts are being focused on the research and development of CMCs with dense matrix and fibre coatings.[2; 6]

In the case of coatings, they should not degrade the mechanical properties of the fibre. Thus, the coatings which react or dissolve the fibres are generally unacceptable and this thermochemical requirement limits the potential of various materials for such applications.[5]

3.2.1. Fibre coating

Various conceptions of coating fibres have been studied.[11] Initially, these concepts involved the use of materials inherently lubricant, such as carbon and boron nitride.[12] They present preferential cleavage planes and usually have layers mutually compatible within each other, thus lowering the roughness between fibre and matrix. These materials, however, did not present good performance due to high susceptibility to oxidation at high temperatures.[13]

Other studies have been developed for the applications of oxide coatings in systems where high oxidation resistance and high thermal stability were desired. Monazite systems, such as $LaPO_4$, YPO_4, among others, have shown to be very promising because of their low interfacial fracture energy, being sufficient to cause crack deflection.[14; 15]

Oxide coatings in the form of layers have also been studied. These layers have high anisotropy of fracture providing preferential cleavage planes. Such compounds include hexa-aluminates β-alumina and magnetoplumbite structures. The hexa-aluminate hibonite ($CaAl_{12}O_{19}$) was considered very promising for application in alumina-alumina CMCs.[16]

Due to the decrease in fracture energy promoted by porosity, porous coatings were studied by He and Hutchinson.[17] It was postulated that cracks are usually deflected connecting pores and hence, imposing less stress concentration in the fibres than in the matrix. Zirconia(ZrO_2), yttria (Y_2O_3) and alumina (Al_2O_3) coatings were studied, but it is necessary that the coating density is well below the theoretical density so that a weak interaction between fibre and matrix is established.[5]

Fugitive coatings, usually based on carbon, were also studied. The term "fugitive" means that the coating material can be removed after

manufacture of the composite, for example by oxidation to form voids (porosity) in the fibre-matrix interface.[2; 11]

3.2.2. Zirconia-based interfaces

The zirconium oxide (ZrO_2), commonly called zirconia, has been studied and used in the production of weak fibre-matrix interfaces.[2; 6; 11]

Carpenter and Bohlen[18] developed a coating process in which metallic zirconium is oxidized *in-situ* producing monoclinic zirconia (unstabilized, m-ZrO_2) around the fibres and thus, during cooling, the volume increases due to the tetragonal $\rightarrow$ monoclinic transformation[19; 20] results in a coating with microcracks. The microcracks present in the fibre-matrix interface assist in mitigating the advance of cracks originating from the matrix.

Davis et al.[5] studied fibre coatings produced via reactive sputtering and unstabilized and stabilized zirconia with yttria (Y_2O_3) in composites with sapphire fibres and polycrystalline alumina (Al_2O_3) matrix. Residual stresses originating from differences in thermal expansion coefficients of zirconia and matrix occurred in both cases and microcracks were observed.

Stempin and Wexell[21] studied fibre coating in glass-ceramic composites reinforced with silicon carbide (SiC) fibres. Two methods were used: the first consisted in coating the fibres with a solution of organometallic zirconium and a subsequent oxidation process for the formation of monoclinic zirconia and the second consisted of coating the fibres with a colloidal solution of zirconia. High damage tolerance of the composites at room and high were reported. Colomban et al.,[22] developed a coating of zirconia in mullite matrix composites with Nextel™ 440 fibres using sol-gel process. Good damage tolerance but relatively low flexural strength (70 MPa) were achieved. Later, Bockmeyerand and Krüger evaluated influences of various kinds of zirconia, such as crystalline, amorphous, stabilized and unstabilized, as well as different precursors on the degradation and loss of mechanical properties on alumina fibres Nextel™ 610.[23] The application of sol-gel techniques for producing zirconia interfaces in SiC/SiC composites was also studied by Utkin et al.[24]

Lee et al.[25] studied oxide multilayer interfaces in Hi-Nicalon™/SiC minicomposites in the following sequence: amorphous silica (SiO_2), monoclinic zirconia (m-ZrO_2) and amorphous silica again. The interface was produced via chemical vapour deposition (CVD). Good mechanical properties and damage tolerance were acquired. The damage tolerance

occurred in part by a weakening of the interface caused by the residual stresses formed by the difference in thermal expansion coefficients of amorphous silica and monoclinic zirconia. From this work, the influence of polymorphism of zirconia on the characteristics of the interface has been extensively studied by Li et al.[26;27]

Gu et al.[28]coated alumina fibre fabrics (Nextel™ 720) via dip-coating with colloidal suspension of nanosized particles of zirconia. Various manufacturing methods and precursors were used. The dip-coating process using zirconia synthesized by hydrothermal process proved to be very efficient (Figure 1).

Figure 1.SEM image showing a zirconia coating (bright region) with 1-2 μm thickness.

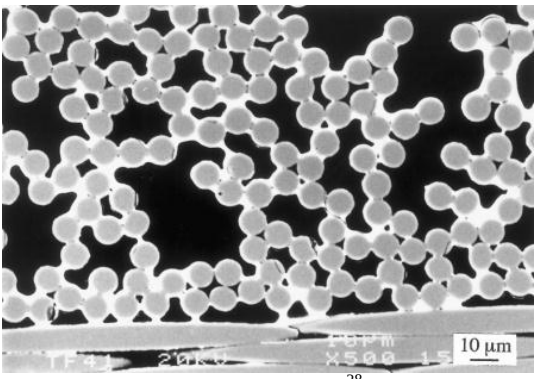

Source: Gu et al.[28]

Parthasarathy et al.[29] have studied a mixture of zirconia, silica and carbon as fibre coating of Nextel™ 720/Blackglas™ minicomposites, thus producing a porous surface primarily caused by oxidation and removal of carbon. Figure 2-a shows Weibull distributions for samples coated with zirconia-silica and without coating. An increase of approximately 90 MPa (34%) can be seen observed and a decrease of the Weibull modulus. Figure 2-b presents the force-displacement curve, showing damage tolerance, e.g., pseudo-plastic fracture caused by toughening mechanisms, which are promoted by weak interfaces. Later, another similar work was developed by Boakye et al.[30]

Figure 2.Minicomposite with zirconia-silica interface. a) Comparison with Weibull distribution of the maximum tensile strength of samples with and without fibre coating b) force-displacement curves.

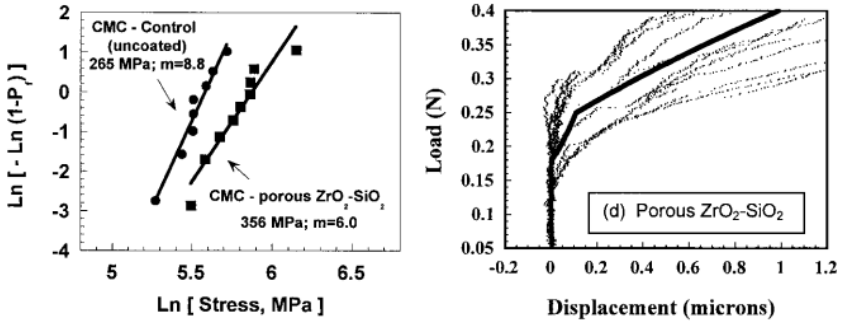

Source: Parthasarathy et al.[29]

3.3. FAILURE PROCESS AND TOUGHENING MECHANISMS OF CMCS

CMCs behave like elastic materials which exhibit non-linear damage (pseudo-plasticity) as shown in Figure 3-a. As the fibres are strongly bonded to the matrix, brittle failure occurs when the composite is loaded in tension, e.g., the stress-strain curve provides linear elastic behaviour up to the point at which a crack propagates through the material.[31] However, as fibres exhibit a relatively weak adhesion to the matrix, instead of a catastrophic failure as the stress limit is reached, microcracks are created and propagate until they deflect at the interface region, leaving the fibres intact and partially or even totally separated from the matrix. This process is called crack deflection.[17] As the crack advances, fibres remain intact carrying the crack opening forces. This phenomenon is called crack bridging.[32; 33] With the increasing tensile load, the fibres begin to fracture randomly, according to the Weibull theory, and energy is spent on friction as fibres are pulled out of the fractured matrix. This phenomenon is called fibre pullout (Figure 3-b).[34] The phenomena mentioned above, such as crack deflection, crack bridging and pullout are considered the main toughening mechanisms in CMCs.[1]

Figure 3. a) Example of stress-strain curves for monolithic ceramics (1) and CMCs (2). b) Process of fracture in CMCs.

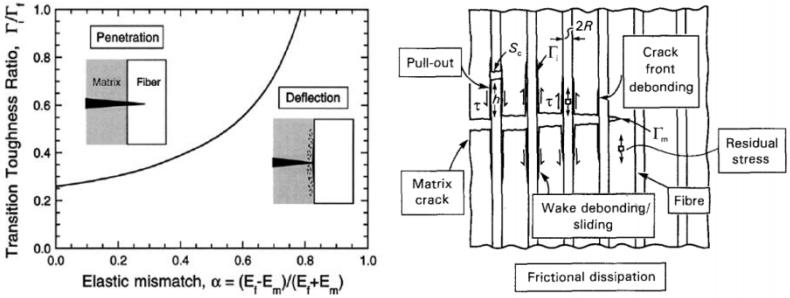

a) Adapted from Krenkel;[2] b) Adapted from Evans and Zok.[35]

3.3.1. Crack deflection

As minimum requirement for damage tolerance in composites reinforced with ceramic fibres, it is preferable that existing cracks in the matrix are blocked or deflected into the fibre-matrix interface rather than penetrated into the fibres. The conditions which meet these requirements were obtained by the work of He and Hutchinson.[17] The diagram that predicts crack deflection is shown in Figure 4. Crack deflection is expected to occur when the ratio of the toughness of the interface Γ_i, and the toughness of the fibre, Γ_f is smaller than the ratio of the energy release rates associated with the crack deflection along the interface, G_d, and penetration into the fibre, G_p, Equation (1). The toughness is calculated according to Equation (2), where K_{IC} is the fracture toughness and E is the elastic modulus of the material in question.

$$\frac{G_d}{G_p} < \frac{\Gamma_i}{\Gamma_f} \qquad 1)$$

$$\Gamma = \frac{{K_{IC}}^2}{\mathrm{E}} \qquad 2)$$

The critical ratio, G_d/G_p, is influenced by the difference of elastic modulus of the fibre and the matrix (or interface) in plane stress state. α is a

dimensionless parameter that relates the difference in modulus between the matrix and fibre, with m and f indices, respectively (Eq. (3)). The difference between the modulus of elasticity generates shear stresses at the interface causing a mixed state of stresses at the crack tip, tensile and shear.[1] The elastic modulus is described in Equation (4).

$$\alpha \equiv \frac{(\overline{\mathrm{E}}_f - \overline{\mathrm{E}}_m)}{(\overline{\mathrm{E}}_f + \overline{\mathrm{E}}_m)} \qquad 3)$$

$$\overline{\mathrm{E}} = \frac{\mathrm{E}}{(1 - v^2)} \qquad 4)$$

The critical condition of fibre and matrix properties can be obtained as follows: for $\alpha \geq 0$, the energy release rate, G_d/G_p can be represented by the empirical equation (5).

$$\frac{G_d}{G_p} = \frac{1}{4(1-\alpha)^{0.9}} \qquad 5)$$

In the extreme situation $G_d/G_p = \Gamma_i/\Gamma_f$ in Eq. (5) and combining with Eq(3) for similar materials, the condition of deflection can be expressed as follows (Eq.(6). Σ is a dimensionless parameter that characterizes the tendency for crack deflection to occur. Another approach for crack deflection taking porosity into account can be found in the literature.[36]

$$\Sigma \equiv 0.134 \left(\frac{\Gamma_f}{\Gamma_i}\right)\left(1 + \frac{E_f}{E_m}\right)^{0.9} \qquad 6)$$

Figure 4.Diagram showing the condition for crack penetration or deflection at the interface.

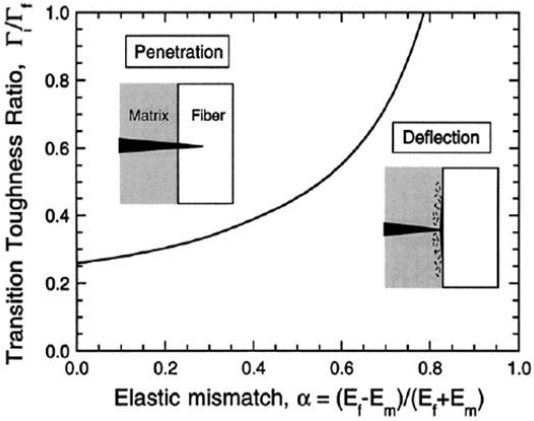

Adaptated from Zok e Levi.[8]

3.4. FIBRE COATING (DIP-COATING)

The dip-coating technique can be described as a process where the substrate to be coated is immersed in a liquid or suspension, and then withdrawn at a well-defined speed. The thickness of the coating is defined mainly by the speed of withdrawal, the amount of the solid content of the suspension and the viscosity of the suspension. If the removal rate is chosen in a way that the shear rate maintains the system under Newtonian regime, the thickness of the coating can be calculated by the Landau-Levich equation (Eq. (7)), where h is the thickness of the coating, η the liquid viscosity, v the withdrawal speed, γ_{LV} the liquid-vapour surface tension, ρ the liquid density and g, gravitational acceleration.[37]

$$h = 0.94 \frac{(\eta.v)^{2/3}}{\gamma_{LV}{}^{1/6}.(\rho.g)^{1/2}} \qquad (7)$$

Figure 5.Schematic showing the dip-coating steps. a) immersion, b) start-up, c) deposition and drainage, d) drainage, e) evaporation and f) continuous process

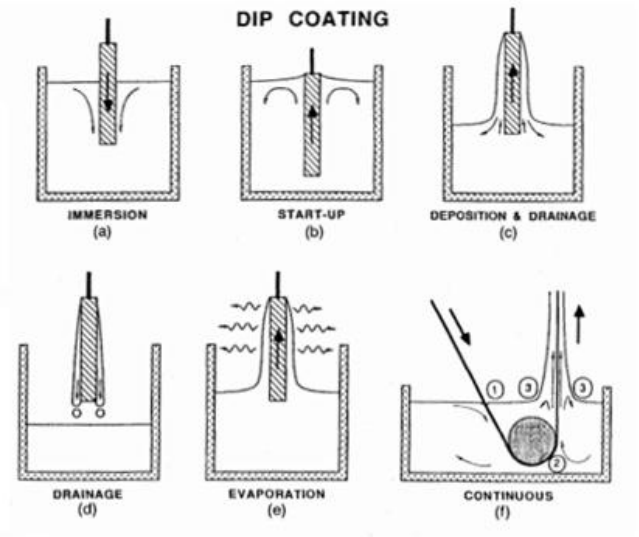

Source: Brinker and Scherer.[37]

3.5. NANOINDENTATION

Nanoindentation is a technique developed during the 80´s to evaluate mechanical properties of materials at very small scales. This technique employs high-resolution sensors and actuators that control continuously loads and displacements during the indentation.[38] In some systems it is possible to have force and displacement measurements in order of nN and Å, respectively. Figure 6 presents an example of a nanoindenter with and schematic of its actuators.

Several mechanical properties can be determined by this method as hardness, elastic modulus, fracture toughness, fracture energy, among others.[39] Due to the high accuracy of such systems, properties such as hardness are measured directly from the load and displacement data, eliminating the need for image analyses.[40] With suitable indenters, it is also possible to make indentations in brittle materials with radial cracks in the contact ends that allow exploring fracture aspects and characteristics of the

material on a microscopic scale such as crack propagation and toughening mechanisms.[38; 41]

Figure 6.Example image (a) and system schematic (b) of a nanoindenter.

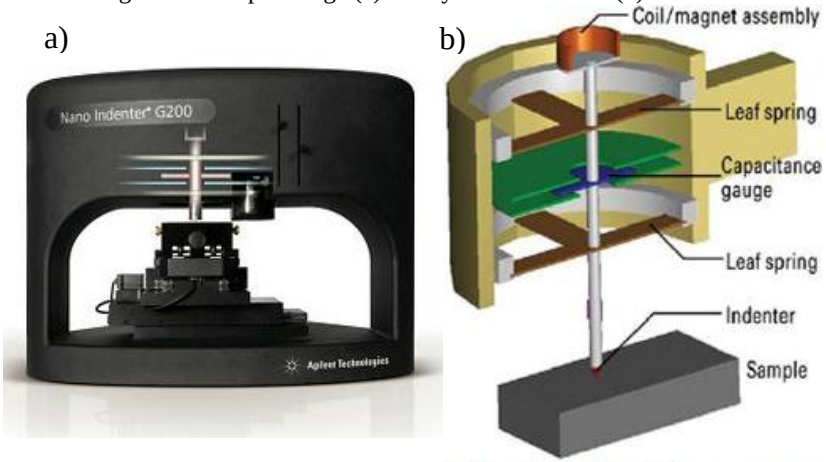

Source: a) Agilent Technologies;[42] b) LY Laboratory Facilities.[43]

3.5.1. Determination of elastic modulus

The elastic modulus can be determined by nanoindentation tests when the indentation load, P, and displacement, h, are continuously registered during the complete cycle of loading and unloading. The rigidity of contact between the indenter and the sample material is required to determine the elastic modulus. Since the loading curve takes into account both elastic and plastic deformations, the stiffness, S, can be determined by the initial slope of the unloading curve. S =dP/dh, and P is described by the relation given by Oliver and Pharr:[44]

$$P = A\,(h_f - h_i)^m \qquad (8)$$

where A and m are regression parameters of the curve, being acquired during the first 65% of the unloading curve, as shown in Figure 7. With the determination of the stiffness S, the reduced elastic modulus, E_r,

can be estimated, which computes the elastic displacement of the material under examination and the indenter in Eq. (9).

$$E_r = \frac{\sqrt{\pi}}{2}\frac{S}{A} \qquad 9\ )$$

The elastic modulus of the material, E_m, can be then calculated using the reduced elastic modulus, according to Eq. (10).

$$\frac{1}{E_r} = \frac{1-\upsilon_m{}^2}{E_m} + \frac{1-\upsilon_{ind}{}^2}{E_{ind}} \qquad 10\ )$$

Where ν_m is the Poisson's ratio of the material, E_{ind} and ν_{ind} are the respective elastic modulus and Poisson's ratio of the indenter, being 1140 GPa and 0.07 for the Berkovich indenter, respectively.

Figure 7.Schematic representation of the load-displacement for a nanoindentation test.

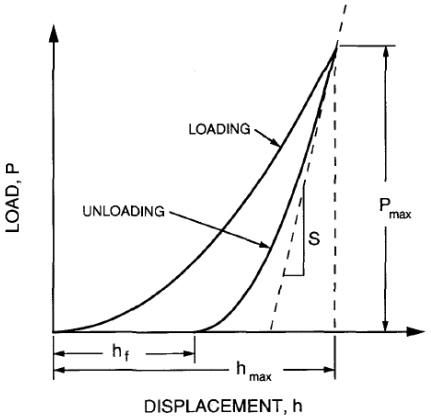

Source: Oliver and Pharr.[44]

3.5.2. Determination of the interfacial sliding stress (fibre pushin)

In order to analyse and compare the performance of the two different monoclinic zirconia fibre-matrix interfaces, the interfacial shear properties were studied. In this case, the test used was a modification of the fibre

pushin first proposed in the work of Marshall and Oliver.[45] This modification, introduced by Weaver et al.[46] presents advantages over the standard method, especially for porous materials, such as porous matrix composites and composites with porous interfaces.

The method uses the loading-unloading hysteresis loop width rather than the absolute displacement to assess the interfacial sliding stress. This eliminates the problem with the high elastic deformation at the interface region during loading, which is given by its relatively low elastic modulus. The loop width is obtained by subtracting the measured displacements on loading and unloading at each load level. All the extraneous displacement is elastic, so it does not contribute to the displacement difference. Also, it is assumed that there is no plastic deformation influencing the test, so a flat conical indenter was used. In this method, each fibre is loaded up and unloaded to a defined load three times, on the first loading cycle, plastic deformation of the indenter on the fibre occurs, so it is not used for interfacial sliding stress calculations. The subsequent two loops are then used for such assessment.

Figure 8 presents an example of the two first hysteresis loops of the pushin test. Equation (11) describes the loop width for the second and third cycles, being Δ_n the difference of displacement for each level of force in one hysteresis loop, Δ_* is the reference displacement described in Equation (12). In Equation (12) F_M is the maximum force, R is the fibre radius, τ is the interfacial sliding stress and E_f the elastic modulus of the fibre. Equation (13) describes the normalized force, being F the force in each loading level. By fitting Equation (11) on the data provided by the hysteresis cycles, the interfacial sliding stress, τ, can be estimated.

$$\frac{\Delta_n}{\Delta_*} = \mathrm{k}(1-\mathrm{k}) \qquad 11)$$

$$\Delta_* \equiv \frac{F_M^2}{(4\pi\, R^3\, \tau\, E_f)} \qquad 12)$$

$$\mathrm{k} = \frac{F}{F_M} \qquad 13)$$

Figure 8.Example of the modified fibre pushin test.

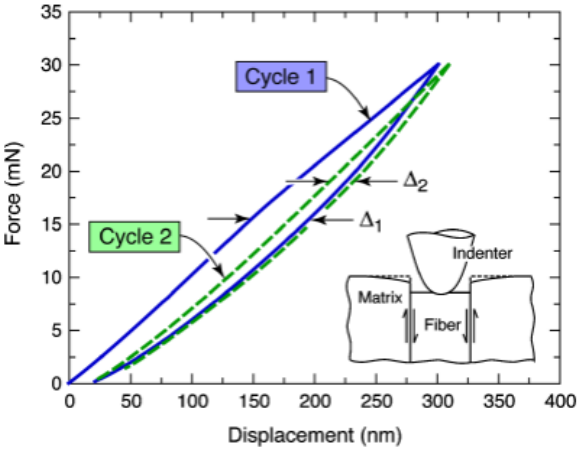

Source: Zok. [47]

3.6. DETERMINATION OF FRACTURE TOUGHNESS

The single-edge-V-notched beam test (SEVNB) is a fracture toughness test based on the single-edge-notched beam (SENB) test.[48] The SENB test, however, has been found to be heavily influenced by the width of the notch root. The SEVNB test was found to be user-friendly, reliable, reproducible and comparable with other standard methods for testing fracture toughness, such as the chevron notch and the single-edge-precracked beam tests. For these reasons, the SEVNB test was chosen as the standard method for determining the mode I fracture toughness (K_{IC}) of the monoclinic zirconia interfaces.

The experiment consists then in bending a bar-shaped specimen having a notch with a tip radius with less than 10 µm, as shown in Figure 9. The fracture toughness can be calculated according to Equations (14) and (15), where K_{IC} is the fracture toughness, F is the maximum bending force, S_1 and S_2 are the outer and inner spans, respectively, α is a/W, a is the crack length, B is the specimen width, W is the specimen height and Y* is the stress intensity shape factor.

$$K_{IC} = \frac{F}{B\sqrt{W}} \frac{S_1 - S_2}{W} \frac{3\sqrt{\alpha}}{2(1-\alpha)^{1.5}} Y^* \quad (14)$$

$$Y^* = 1.9887 - 1.32\alpha - (3.49 - 0.68\alpha + 1.35\alpha^2)\alpha(1 - \alpha)(1 + \alpha)^{-2} \quad (15)$$

Figure 9. Schematic of the SEVNB specimen: a) Common test configuration b) detail of the notch characteristics.

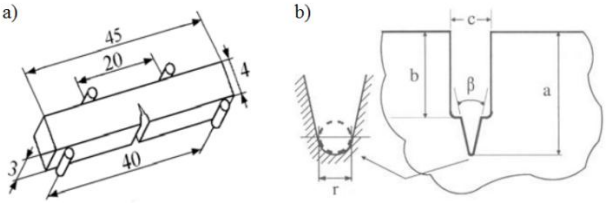

Source: a) Powder metallurgy and metal ceramics.[49] b) Kubler.[48]

4. MATERIALS AND EXPERIMENTAL PROCEDURE

4.1. MATERIALS

In the present work alumina-alumina composites with monoclinic zirconia fibre-matrix interfaces were produced. The materials used were: polycrystalline alumina fibres, dense matrix produced using submicrometric alumina powder and fibre-matrix interface produced via dip-coating single fibres in suspensions of monoclinic zirconia, in order to create a porous and weak interface.

4.1.1. Fibres

Model composite were fabricated using Nextel^{TM} 610 fibres, supplied by 3M (Germany). These oxide fibres consist mainly of polycrystalline α-alumina with an average grain size of 80 nm. They present high tensile strength; however, present low creep resistance at temperatures higher than 1100 ºC[50] due to the strong grain growth.[51; 52] Table 1 shows the main properties and Figure 10 presents a SEM image of the Nextel^{TM} 610 fibres.

The fibres used were extracted from bundles (rovings) with ~400 filaments per bundle (1500 denier).

Table 1.Properties of the Nextel^{TM}610 fibres.[53; 54]

Composition	> 99.99 % α-Al_2O_3
Average tensile strength (MPa)	3200
Weibull modulus	10-12
Elastic modulus (GPa)	372
Density (g/cm³)	3.82
Diameter (μm)	11.64
Thermal expansion coefficient (K^{-1})	7.1 x 10^{-6}
Poisson's ratio	0.27

Figure 10.3M Nextel™ 610 fibre.

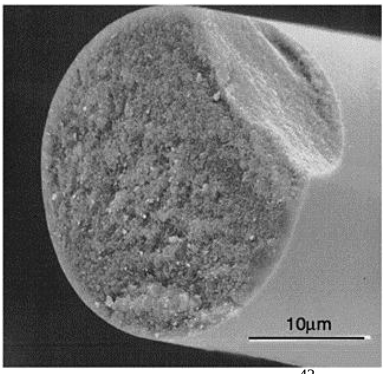

Source: 3M Company.[42]

4.1.2. Matrix

The material used as matrix was high purity submicrometric alumina powder Taimicron TM-DAR provided by Taimei (Japan), with an average particle size of 0.1 µm, which allows high densification at temperatures < 1350 °C.[55; 56] Table 2 describes the main properties of Taimicron TM-DAR alumina powder.

Table 2.Properties of the Taimicron TM-DAR alumina.[55]

Crystalline form	Alfa (α)
Purity (%)	> 99.99
Specific surface area (m^2/g)	9.0
Average particle size (µm)	0.2
Density after pressing (g/cm^3)	2.3
Density after sintering (g/cm^3)	3.93

4.1.3. Fibre-matrix interface

Monoclinic zirconia was used for the production of the fibre-matrix interfaces. Two different powders were used: the first presented a relatively small mean particle size, of about 0.15 µm, supplied by (Sigma-Aldrich, Germany). The second powder presented a larger mean particle size, of about 0.80 µm (SF-Extra, Carpenter Engineered Products, USA). First,

mixtures of monoclinic zirconia (0.15 µm) and alumina powder (0.1 µm) were tested, although presented high densities and high affinity with the alumina fibres. In addition, monoclinic zirconia powder with particle sizes of 3 and 6 µm were tested, although did not present good properties for the preparation of dip-coating suspensions.

Monoclinic-zirconia was employed in the production of interfaces due to microcracking mechanism caused by the tetragonal → monoclinic phase transformation with an increase of approximately 4% of the unit cell.[5] Moreover, zirconia presents no reaction with alumina to a temperature up to about 1900 °C in any proportion, as shown in the phase diagram in Figure 11. Therefore, it is possible to achieve good porosity due to the zirconia powder particle sizes and also reduce the chemical interaction between the material and the fibre interface.

Figure 11. Alumina-zirconia phase diagram showing that no chemical reaction occurs in temperatures up to 1900 °C.

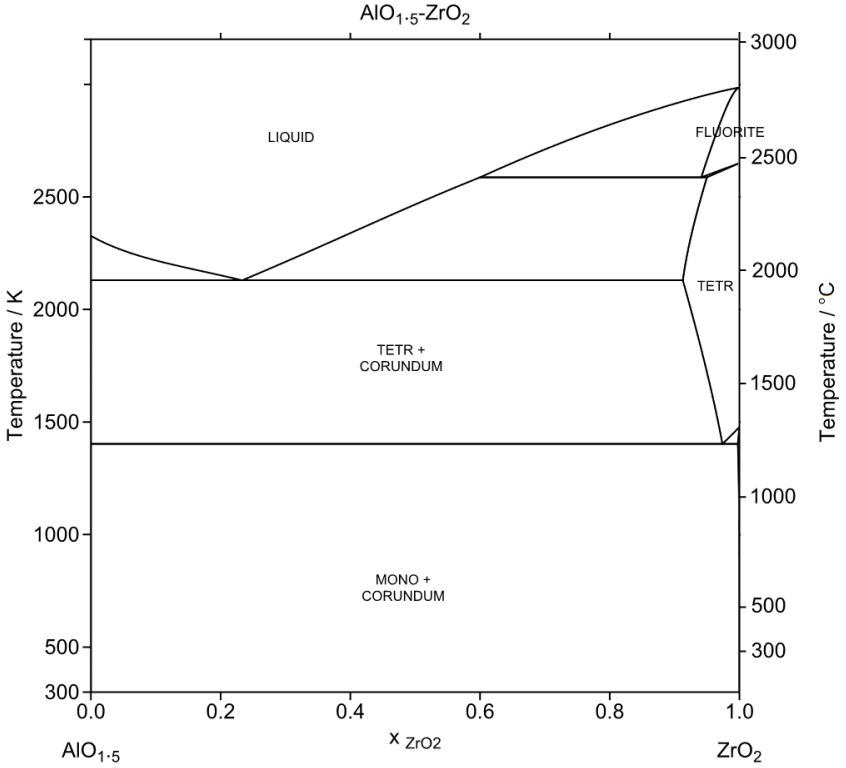

Source: Adapted from MTDATA Software.[42]

4.2. SAMPLE PREPARATION

4.2.1. Fibre dip-coating

The fibre-matrix interface was produced by coating single fibres with a ceramic suspension via dip-coating (Section 3.4). Variations of coating`s particle size and their composition are presented in Table 3. The dip-coating suspensions were produced by attrition milling for 15 minutes with a rotation speed of 500 rpm. Zirconia balls were used as milling media.

The dip-coating suspension had its solid content varied according to the particle size of the powder (see Table 3) and were prepared using distilled water and dispersed with Dolapix CE 64 (Zschimmer and Schwarz, Germany) at 1%wt of the amount of powder. The solid content was optimized in order to achieve an adequate coating thickness. It was seen that by increasing the amount of solids, the coating thickness did not change significantly.

Table 3.Dip-coating suspension parameters.

Denomination	Ceramic powder	vol% of solids	Dispersant
Z015	m-ZrO2 (0.15 μm)	55	1 wt%
Z080	m-ZrO2 (0.80 μm)	45	1 wt%
NC	Absence of coating	--	--

Fibres were first desized in a muffle furnace at 500 °C for 2 hours and then coated as shown schematically in Figure 12. The ceramic suspension was put in a watch glass and single fibres were manually immersed in the suspension and then withdrawed sideways at a constant rate to achieve a uniform coating.

Figure 12. Schematic of the dip-coating procedure

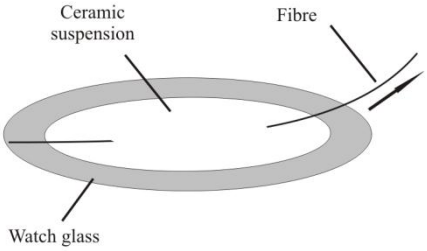

4.2.2. Production of model composites

Dip-coated fibres were laid in the middle of an alumina powder bed and pressed in order to produce model composites (see Figure 13). A

rectangular compaction mould (47x7x5 mm^3) was filled with half of the necessary amount of alumina powder and then the powder surface was flattened in order to create a substrate for the coated single fibres. Over the flattened powder, 10 to 15 coated fibres were placed and the mould was then filled with the other half of powder. This process guaranteed the fibres to be in the middle plane, ensuring the position and facilitating the localization of the fibres inside de model composite (see Figure 13).Samples were uniaxially pressed at 30 MPa and then pressed isostatically at 300 MPa and sintered for 1 hour at 1350 °C using a heating rate of at a 3 °C/min.[57]

Figure 13.Schematic of the model composite preparation.

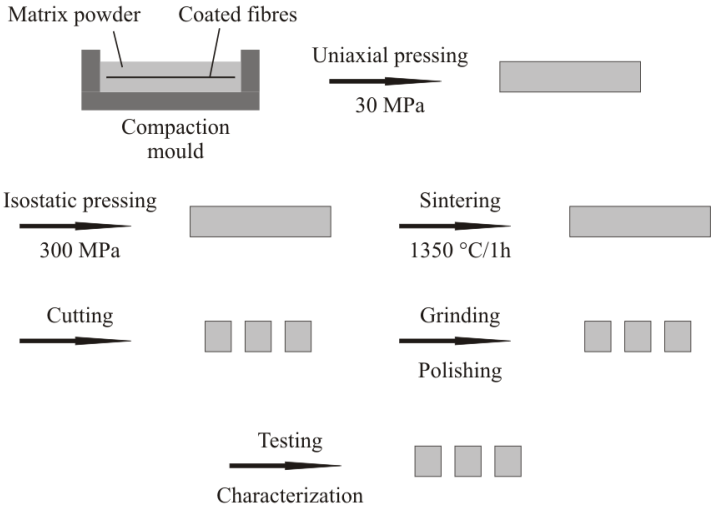

4.2.3. Production crack deflection specimens

The specimens used for the evaluation of the crack deflection mechanism were produced by cutting 1.5 mm thick transversal slices of the sintered model composite bars. The cuts were made using a diamond cutting saw (MCPEXAKT-Apparatebau, No. 60/13, Germany) with a turning speed of 3600 rpm. The specimens for crack deflection observations were embedded in epoxy resin and subsequently polished using

conventional polishing methods up to 0.25 µm particle sized diamond suspension. The epoxy resin was burned out at 700 °C for 2 hours.

4.2.4. Production of fibre pushin test specimens

The specimens used for the fibre pushin test were produced in similar manner as for the crack deflection test. The, thickness however, was chosen to be 0.5 mm, as suggested in the literature.[46]

4.2.5. Production fibre pullout specimens

The pullout mechanism was evaluated by testing model composite bars in 4-point-bending and later observing, via scanning electronic microscopy (SEM), the fracture surface. The test was performed by bending notched model composite bars in order to specify the failure location.

4.3. CHARACTERIZATION

4.3.1. Powder particle size

The particle size was determined via scanning electron microscopy for small particle sizes below 0.5 µm in order to achieve more precision. For all particle and grain size measurements, the image analysis software (ImageJ) was utilized. The measurements were made semi-automatically. The grains and particles were identified manually and the size was determined automatically.

Particles with more than 0.5 µm were also tested using a laser scattering method. The scanning electronic microscope was a GEMINI / Zeiss, Leo 1530 FESEM, Germany, and the laser scattering equipment was a Malvern Instruments, Germany, with maximum power of 5 mV and He-Ne laser with wavelength of 632.8 nm).

4.3.2. Powder density (true density)

The density of the ceramic powders was determined via helium picnometry with a1305 Micromeritics helium pycnometer. The density measurement was performed 10 times for each sample.

4.3.3. Chemical composition (X-ray diffraction)

The chemical composition of the ceramic powders used in this work was determined via x-ray diffraction. The equipment used was the XRD Siemens, Germany utilizing Cu-Kα radiation.

4.3.4. Bulk density

The bulk density of the matrix and the fibre-matrix interfaces after sintering were determined geometrically using paquimeter and micrometer in rectangular bodies with the respective composition.

4.3.5. Grain size

The grain size of the model composite components (matrix, fibre and fibre-matrix interfaces) was determined using scanning electron microscope images (GEMINI / Zeiss, Leo 1530 FESEM, Germany). The samples were prepared by conventional polishing and chemically etched by polishing with OP-S (silica colloidal suspension) for 15 min and thermally etched submitting the samples to a rapid firing in a temperature 100 °C below the sintering temperature, e.g., 1250 °C/15 min.

4.3.6. Elastic modulus

The elastic modulus of the model composite components was determined via nanoindentation as shown in Section 3.5.1. The test was performed using a calibrated Berkovich indenter. The loading rate was 5 mN/s and the maximum indentation depth varied depending on the material, being 1100 nm for the matrix and fibres and 2000 nm for the interface materials. For each material, 30 indentations were made.

4.3.7. Fracture toughness

The fracture toughness of the dense alumina matrix and fibres was based on literature results. The fracture toughness of the porous monoclinic interfaces was estimated from rectangular bodies via the single edge v-notched beam test (Section 3.6). Bending bars with dimensions of about 3x6x38 mm^3 were also produced according to the schematic shown in Figure 13. These bars were then pre-notched using a diamond disc saw

MCP up to a crack length of 0.6 the thickness. Then the notch was sharpened using a blade runner device (razor blade)[58] for a notch radius under 10 μm to be achieved. The notched specimens were tested in an in-house made displacement controlled four-point bending device[59] with a loading speed of 0.5 mm/s.

4.3.8. Crack deflection

Crack deflection was determined from cracks originated or cracks created by performing Vickers indentations in the vicinity of the fibres. A crack generated by the indentation shall advance towards the fibre perpendicular to the fibre direction. The indentations were performed using a UHL UMTH, Walter UHL (Germany) semi-automatic micro-Vickers indenter. The load used was 19.64 N (machine standard) and was applied on the sample for 10 s. About 10 fibres were tested for each interface composition.

4.3.9. Interfacial sliding stress (fibre pushin)

The interfacial sliding stress was estimated using a modified version of the fibre pushin as already described in Section 3.5.2. The test was performed with a nanoindenter Agilent G200 (USA). The maximum force used for the test was 60 mN and three loading-unloading cycles were made on each of a total of 10 fibres for both interface compositions. The loading rate was 10 mN/s.

5. RESULTS AND DISCUSSION

5.1. MATERIAL CHARACTERIZATION

5.1.1. Matrix

5.1.1.1. Particle size

The particle size of the Taimicron TM-DAR alumina powder was determined via scanning electron microscopy and compared with the data provided by the supplier. Figure 14 shows that the average particle size is about 100 nm, confirming the specification. Also, the figure shows that the powder is rather round-shaped favouring densification during sintering.

Figure 14.SEM image of the alumina powder.

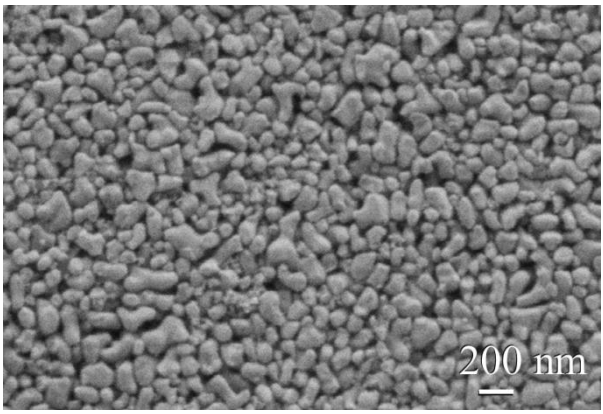

5.1.1.2. Powder density (true density)

The powder density was determined via helium pycnometry in order to precise the matrix porosity estimation. In order to accurate the results the test was performed 10 times. The average density and standard deviation were 3.9955 ± 0.0062 g/cm³.

5.1.1.3.Density and porosity (sintered body)

The relative density of the sintered body was determined by geometrical method and its average is 97 ± 1 %. Fifteen specimens were tested.

5.1.1.4.Grain Size

The grain size was characterized using electronic microscopy. The average grain size of the matrix is approximately 1 µm, as shown in Figure 15.

Figure 15.SEM image presenting the grain size of the alumina matrix.

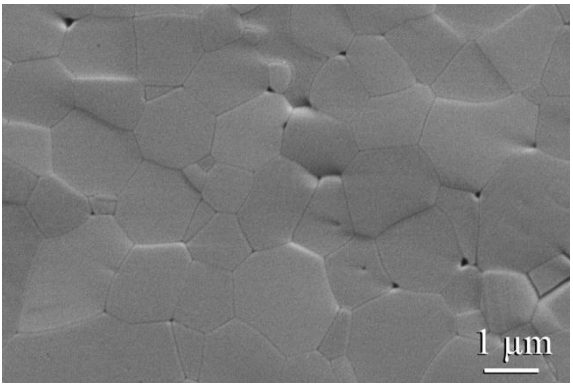

5.1.1.5.Elastic Modulus

The elastic modulus of the alumina matrix was determined via nanoindentation. The test was performed in 30 different locations. The average elastic modulus was 429 ± 14 GPa. The values are similar to those found in the literature (400-440 GPa),[60;61] especially for low depth indentations. An example of a nanoindentation curve for determination of elastic modulus is presented in Figure 16.

Figure 16.Example curve of an elastic modulus determination on the alumina matrix.

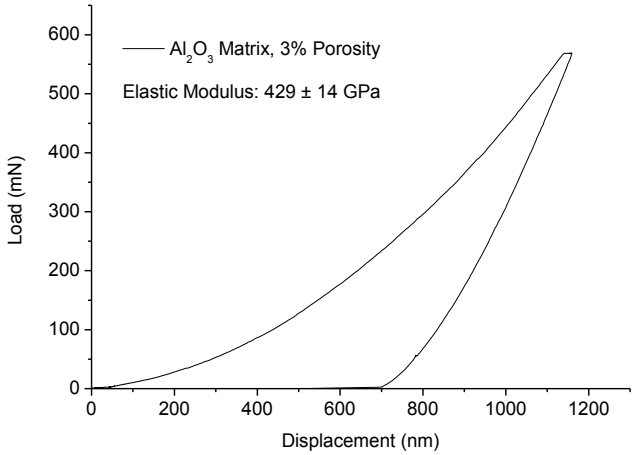

5.1.1.6.Fracture toughness (K_{IC})

The fracture toughness of the dense alumina matrix was found to be 2.5 ± 0.1 MPa.m$^{1/2}$. This value is presented in the literature for similar material sintered at the same temperature, 1350 °C.[53]

5.1.2. Fibres

5.1.2.1.Grain size

The mean grain size diameter of the fibres was determined via scanning electron microscopy. Figure 17 a) shows the microstructure a fibre calcinated at 1100°C/30min used for comparison. No grain growth was observed when compared to the grain size provided by the supplier (~ 80 nm). Figure 17 b) presents a grain size in a 100-400 nm range for a calcination temperature of 1350 °C. The larger grains present epitaxial growth which leads to a decrease of fibre strength.[62] However, for the purpose of this work, this phenomenon is not taken into account.

Figure 17.SEM images showing the microstructure of fibres calcinated at 1100 °C/30 min (a) and 1350 °C /1h (b).

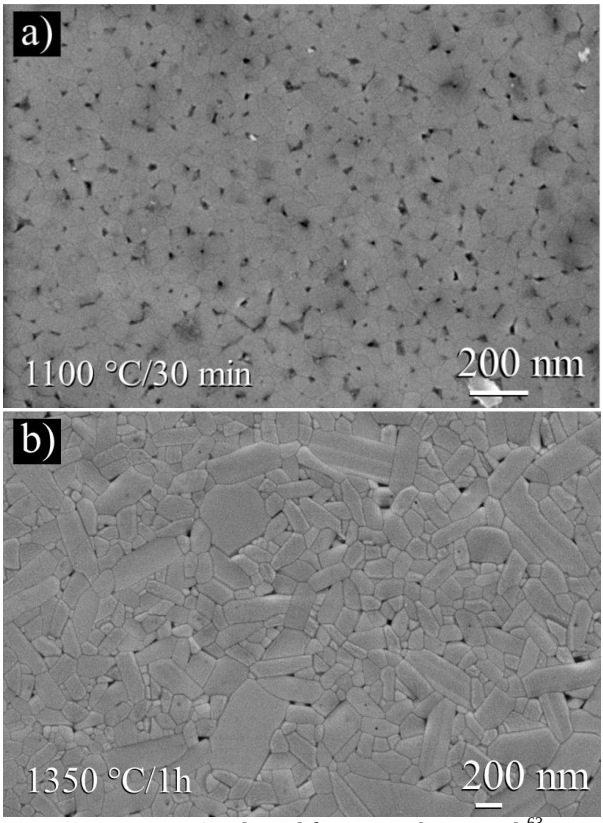

Source: Fig. a) Adapted from Goushegir et al.[63]

5.1.2.2. Elastic modulus

The elastic modulus of the Nextel 610 fibres determined via nanoindentation has an average of 420 ± 15 GPa, which corresponds to the elastic modulus of the dense alumina matrix. An example curve is shown in Figure 18.

Figure 18.Demonstrative curve of the elastic modulus determination using a nanoindenter.

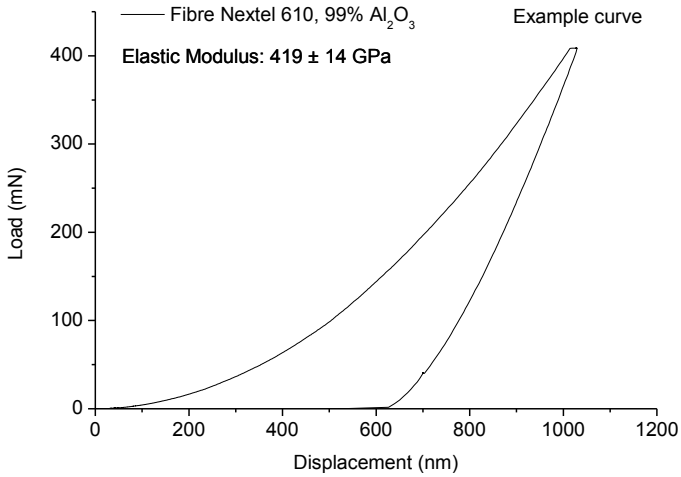

5.1.2.3. Fracture toughness

The fracture toughness of the fibres is 3.7 $MPa.m^{1/2}$. The value is based on a publication dealing with fracture toughness and crack deflection calculations for Nextel 610 fibres.[63]

5.1.3. Fibre-matrix interfaces (monoclinic zirconia)

5.1.3.1.Particle size

The particle size was measured via electronic microscopy and compared to the size given by the suppliers. Results are summarized in Table 4 and are denominated Z015 and Z080 for the 0.15 and 0.80 µm mean particle sizes, respectively. Figure 19 a) presents a SEM image of the Z015 monoclinic zirconia showing a rather uniform particle size of about 0.1 µm. Figure 19b) presents a SEM image of the Z080 particles with have dendritic shape due to a different synthesis method, making it difficult to estimate precisely its mean particle size. In this case, a laser scattering measurement was performed, as described in Section 4.3.1. Figure 20

presents the Z080 particle size distribution. The laser scattering method could not be used for the Z015 powder due to the low resolution for such particle size. The curve confirms the particle size estimated given by the supplier. The second peak present in the graph represents an agglomeration of the powder during the measurements.

Table 4.Meanparticle sizes of the dip-coating zirconia powders.

Denomination	Zirconia powder	Particle size,Supplier(μm)	Particle size, SEM(μm)
Z015	m-ZrO2	< 5	~ 0.10
Z080	m-ZrO2	0.77	~ 0.80

Figure 19. SEM images showing monoclinic zirconia used in the dip-coating suspensions.a) Z015 and b) Z080.

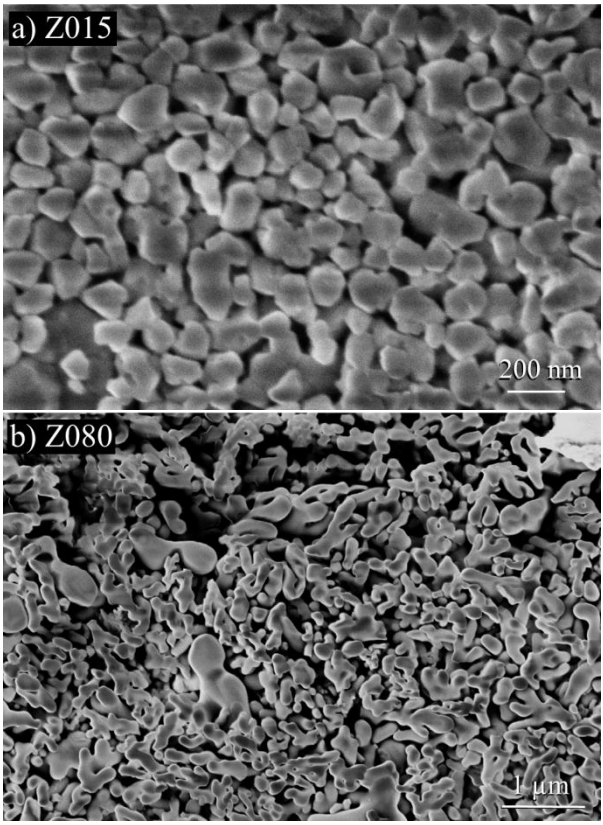

Figure 20.Particle size distribution of the Z080 powder.

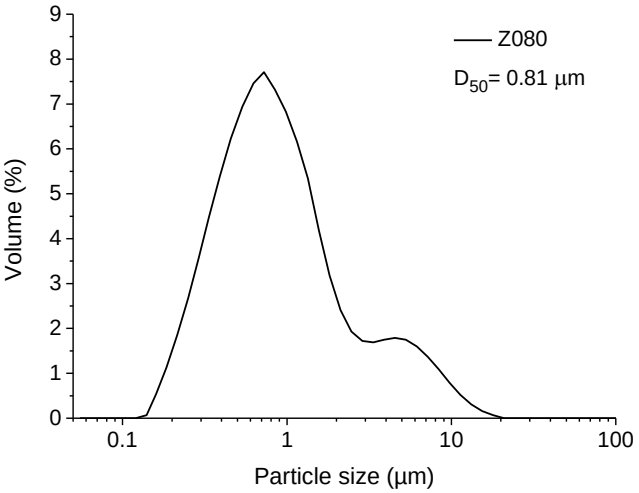

5.1.3.2.Powder density (true density)

The true density of the interface (dip-coating) powders was also measured via helium pycnometry. The results are show in Table 5.

Table 5.Density values for the monoclinic zirconia used in the interface

Denomination	Zirconia powder	Density (g/cm³)
Z015	m-ZrO2	6.05 ± 0.11
Z080	m-ZrO2	6.05 ± 0.02

5.1.3.3. X-ray diffraction

The powder was analysed via X-ray diffraction to confirm its chemical composition. As it is shown in Figure 21, the main peaks match the monoclinic-zirconia pattern.

Figure 21.X-ray diffraction diagrams for monoclinic zirconia powders.

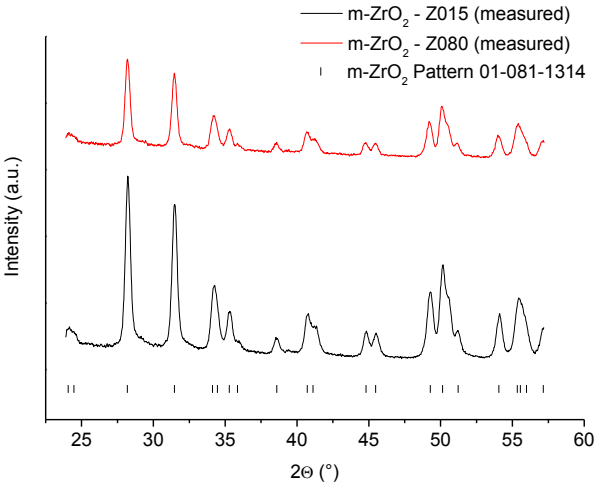

5.1.3.4.Density and porosity (sintered body)

The density and porosity of the interface were estimated from rectangular bodies produced with the monoclinic zirconia powders. The density, therefore the porosity, was determined geometrically. Both materials showed relatively high porosity due to low sinterability. SEM images are shown in Figure 22. a) presents a relatively large amount of intergranular cracks for the Z015 coating. This phenomenon is already predicted by the literature, as reviewed in Section 3.2.2. Larger grain size can be seen for the Z015 interface and this can be explained by the round particle shape and size supporting higher densification levels.

Table 6.Density and porosity of the interface compositions.

Denomination	Zirconia powder	Density (g/cm³)	Porosity (%)
Z015	m-ZrO2 (0.15 µm)	4.04 ± 0.06	30.8 ± 1.0
Z080	m-ZrO2 (0.80 µm)	3.34 ± 0.06	42.8 ± 1.0

Figure 22.SEM images of the zirconia bodies.a) Z015 and b) Z080.

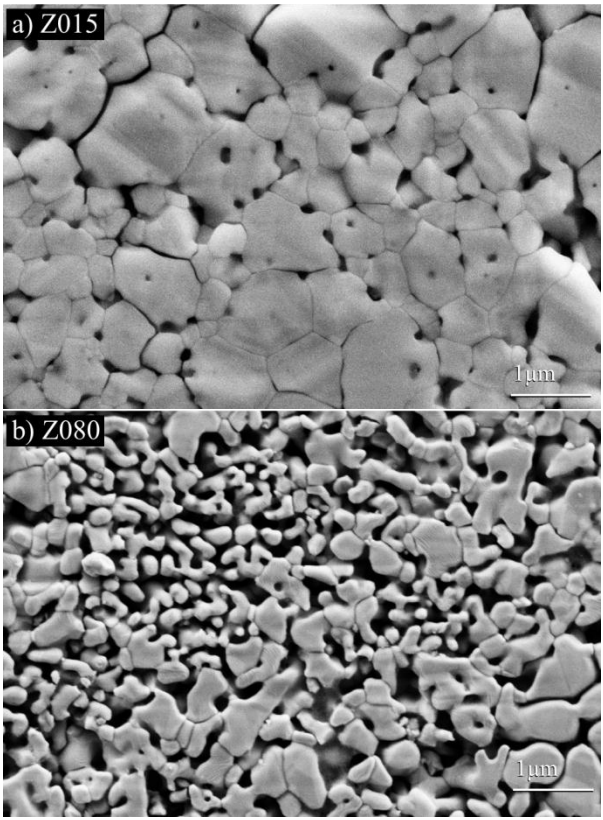

5.1.3.5.Elastic Modulus

The elastic modulus of the monoclinic zirconia was determined also via nanoindentation. The results are presented in Table 7. Composition Z015 showed an elastic modulus of about 34 GPa and the Z080 showed an elastic modulus of about 44 GPa. Despite the fact that Z080 presents higher porosity, it showed higher elastic modulus. This phenomenon can be explained by the presence of a larger amount of intergranular cracks in Z015, increasing its compliance.

Table 7.Elastic modulus and hardness of the zirconia interfaces.

Denomination	Zirconia powder	Elastic Modulus (GPa)	Hardness (GPa)
Z015	m-ZrO2 (0.15 µm)	34.4 ± 4.8	0.92 ± 0.16
Z080	m-ZrO2 (0.80 µm)	43.7 ± 2.5	1.08 ± 0.14

Figure 23.Example of the elastic modulus measurement curve performed via nanoindentation.

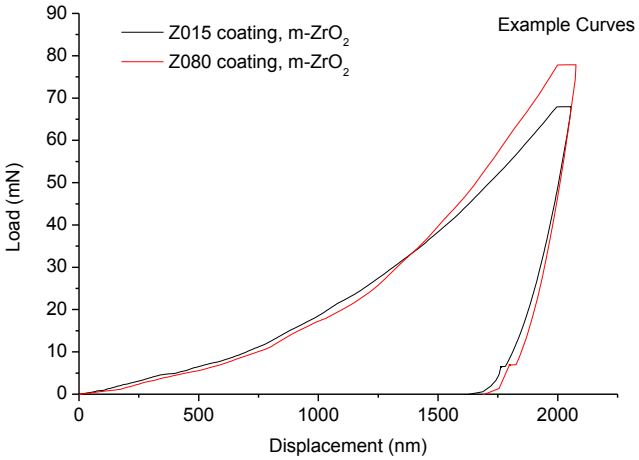

5.1.3.6.Fracture Toughness

The fracture toughness was determined using the SEVNB test. The results are shown in Table 8. This method showed to be very reliable for this material. As shown by the low scattering of the results. The fracture toughness of the Z015 showed to be 28% higher than the Z080 and this can be explained by the higher density of the Z015. Both interfaces present relatively low fracture toughness and so, low fracture energy, which is a requirement for crack deflection. An example curve of the test is shown in Figure 24.

Table 8. Fracture toughness of the monoclinic zirconia interfaces.

Denomination	Zirconia powder	Fracture toughness ($MPa.m^{1/2}$)
Z015	m-ZrO2 (0.15 µm)	0.73 ± 0.02
Z080	m-ZrO2 (0.80 µm)	0.57 ± 0.04

Figure 24.Example curve of the SENVB test.

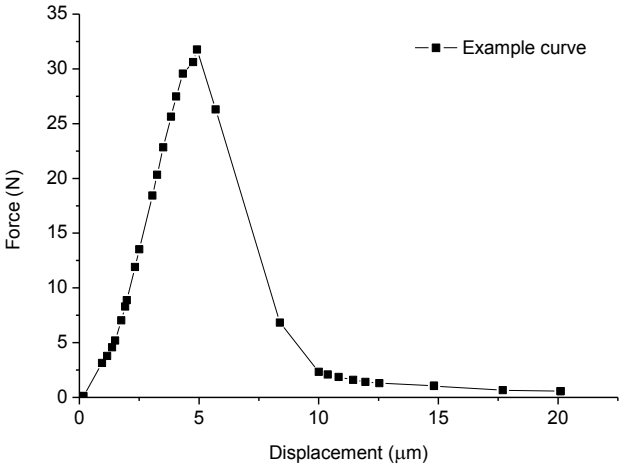

5.2. INTERFACE CHARACTERIZATION

5.2.1. Fibre coating

The coating quality was analysed for coated fibres before sintering. Dip coating generated uniform coatings as well as similar coating thicknesses independent of the coating particle sizes. Figure 25 a) presents a SEM image of the fibre coating and its thickness (~ 1.4 µm) for the Z015 composition. For this estimation, a mean fibre diameter of 11 µm is assumed, taking into account that the fibre diameter varies between 10 and 12 µm. Figure 25b) presents a SEM image for the Z080 coating, which shows also a uniform coating with ~ 0.9 µm thickness. The protuberances shown in both images are originated possibly by powder

agglomeration during processing. The overall coating thicknesses are presented in Table 9.

Table 9.Summary of the mean dip-coating thickness

Denomination	Zirconia powder	Thickness (µm)
Z015	m-ZrO2 (0.15 µm)	1.25 ± 0.50
Z080	m-ZrO2 (0.80 µm)	1.50 ± 0.50

Figure 25.SEM image of dip coated fibres. a) Z015 and b) Z080

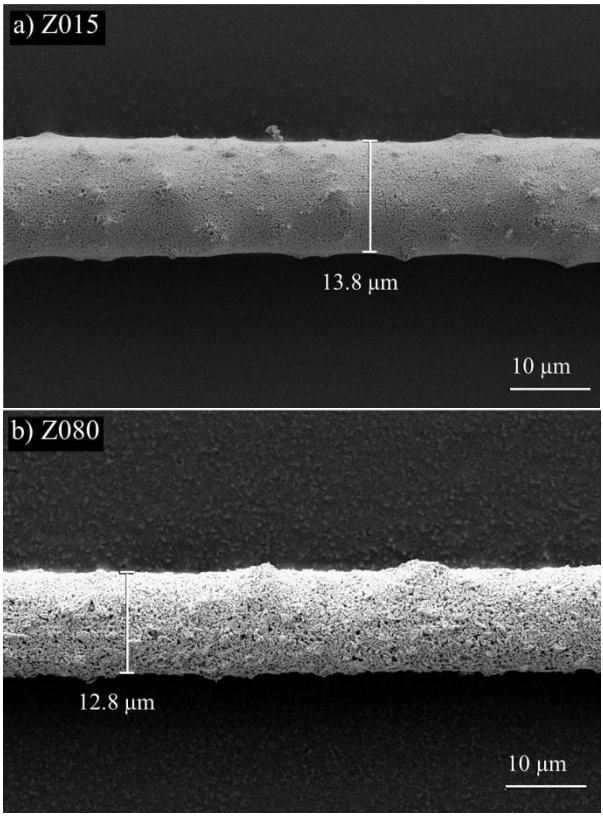

The cross section of the model composites showing both interfaces after sintering is shown in Figure 26 and Figure 27. Figure 26 a) presents the Z015 interface which shows homogeneous coating thickness after sintering. Figure 26 b) shows the interface in more detail. The mean grain size is presented in the 0.5-1 µm range. Figure 27 a) presents the Z080 coating with a relatively high porosity as expected for this particle size. A 1-1.5 µm thickness along the entire fibre circumference is shown. Figure 27 b) shows the interface in detail.

Comparing both coatings, the Z015 is seen to be denser than the Z080 when comparing the images of both coatings alone in Figure 22. This can be explained by the particle shape. The Z015 coating present more round particles than the Z080. Part of the high densification degree of the coating around the fibre is given by the contraction of the matrix during the sintering process. The coating density after sintering was not determined due to difficulties in such determination.

In addition, for both coatings, matrix porosity can be seen around the fibre. This phenomenon is explained by the relatively poor arrangement of the matrix particles around the fibre, thus, leading to an even weaker interface and promoting better toughening mechanisms.

Figure 26. SEM images of the Z015 fibre-matrix interface in the sintered model composite.

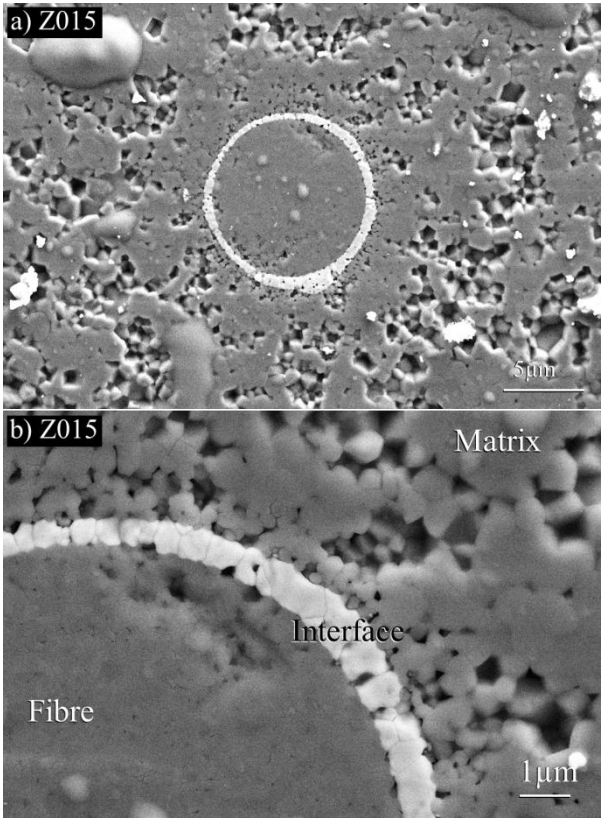

Figure 27.SEM images of the Z080 fibre-matrix interface in the sintered model composite.

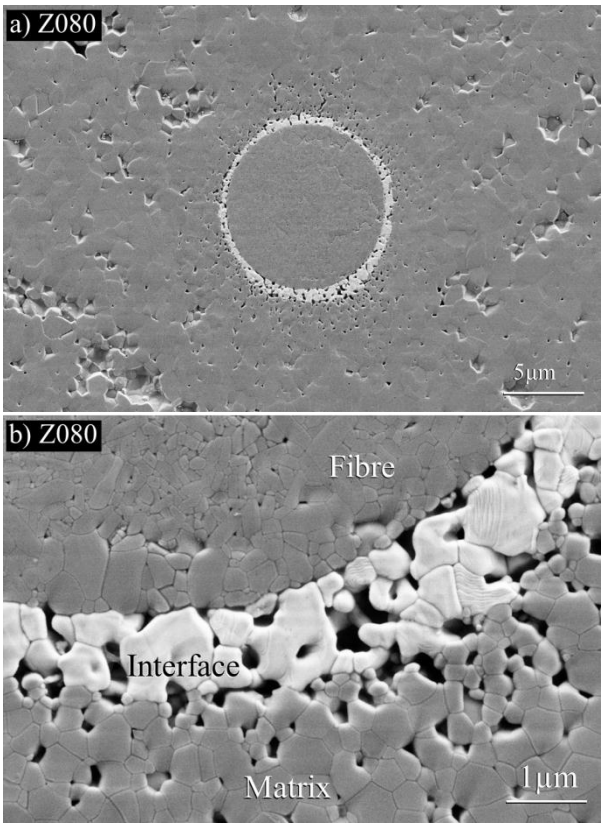

5.2.2. Crack deflection

Crack deflection was evaluated for both interfaces as well as for model composites with the absence of fibre-matrix interface. The qualitative evaluation was performed as detailed in section 4.3.8.Figure 28a) shows a Vickers indentation at the vicinity of the Z015 coated fibre. The generated crack goes towards the fibre and is deflected at the interface, leaving the fibre intact. Crack deflects at the fibre-interface region (at the fibre-interface, Figure 28 b). This shows that low interaction between coating and fibre is present. This phenomenon could prevent the reduction

of fibre strength due to chemical diffusion from fibre to interface and vice versa. In Figure 28 c) multiple cracks can be seen and explained probably by the intergranular cracking. This phenomenon presents once the low fracture energy required by fibre-matrix interface materials. Figure 29 a) presents a Vickers indentation in the vicinity of the Z080 coated fibre. The crack is also deflected, leaving the fibre intact, showing that the main interface requirement is attended. In this case, the crack also goes along the fibre-coating region, showing that low chemical affinity between fibre and coating exists.

Figure 28.SEM images of the crack deflection test for the Z015 coating.

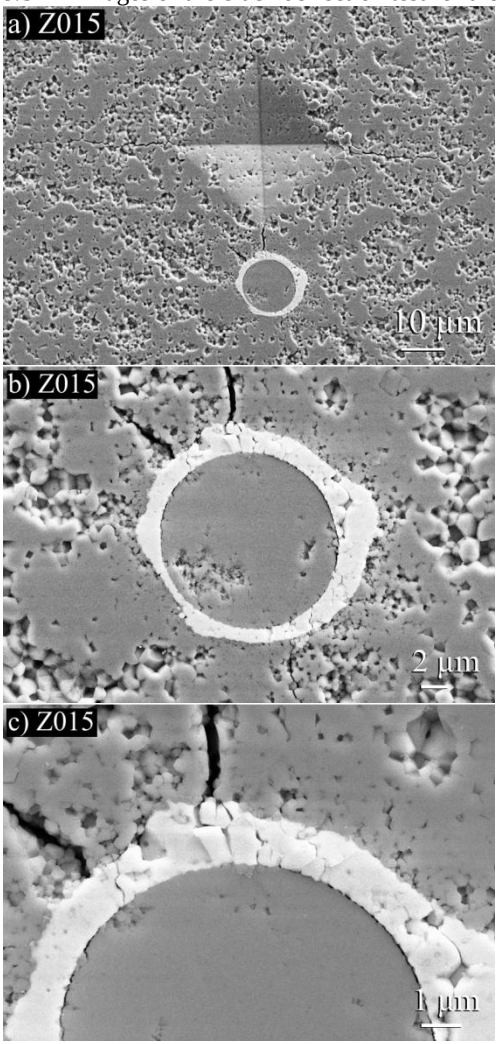

Figure 29. SEM images of the crack deflection test for the Z080 coating.

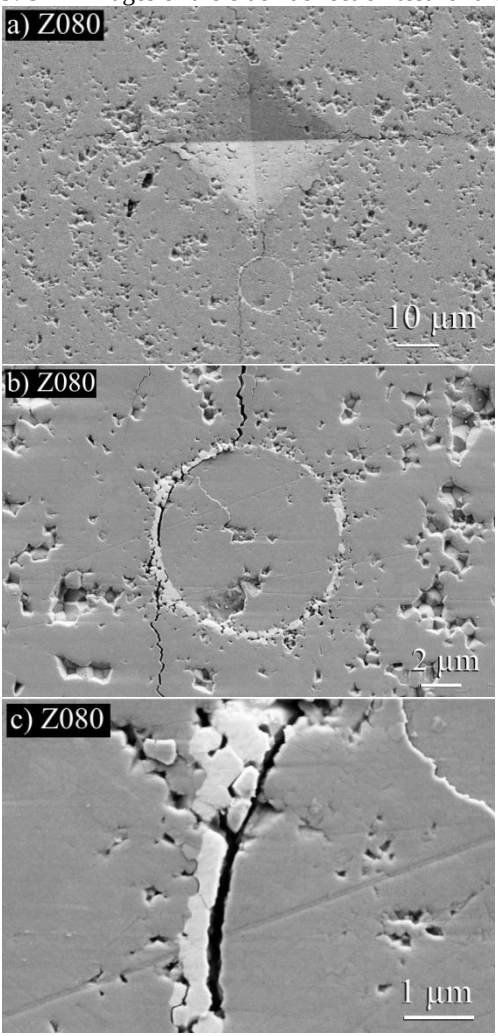

The crack deflection was also performed in model composites without fibre coating. Figure 30 presents a Vickers indentation creating a crack that advances towards an uncoated fibre. The crack penetrates into the fibre. This shows that the absence of monoclinic zirconia interface creates a composite without any toughening. In this situation the failure of the

composite is expected to be catastrophically, similar to a monolithic ceramic. In addition, with absence of interface, the reduction in fibre strength shall be greater than for the coated fibres due to SiO_2chemical diffusion. Nextel 610 fibres contain 0.2-0.3% of SiO_2 to reduce grain growth and it was already shown that SiO_2 diffuses to the matrix at high temperatures, thus, increasing grain growth of the fibres.[64]

The crack deflection behaviour can be proven theoretically using material properties and the diagram published by He and Hutchinson.[17] The elastic modulus and the fracture toughness of the interface, matrix and fibre are needed. Figure 31 presents the theoretical crack deflection criteria for the fibre-matrix interfaces presented in this work. The results are compared with the experimental results provided by the crack deflection test performed by Vickers indentations. As already analysed, both interfaces provide crack deflection behaviour for a crack advancing towards the fibre. The interfaces Z015 and Z080 are placed in the deflection region of the diagram which agrees with experimental results. It can be seen that the Z080 interface is comprehended in a more conservative position that the Z015 coating. This is explained by its lower fracture toughness and consequently, its lower fracture energy compared to the Z015 coating. With the absence of fibre coating, the composite presents no capability of deflection crack around the fibre, and this is also shown in the diagram for the NC (no coating) interface. The NC interface is located well into the crack penetration region, which also is seen in the crack deflection tests based on Vickers indentations.

.

Figure 30. SEM images of the crack deflection test for a NC sample (absence of coating).

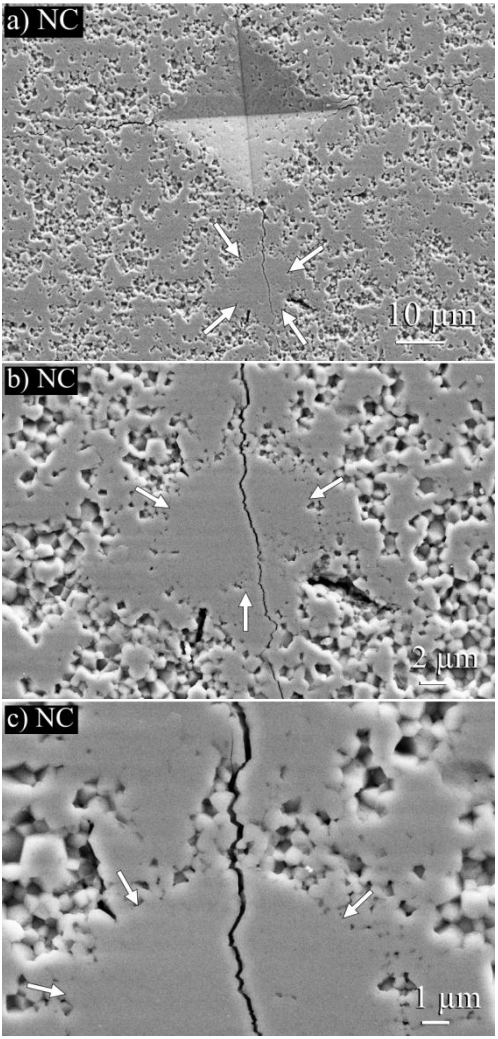

Figure 31. Crack deflection criteria according to He and Hutchison's theory for the Z015, Z080 and NC interfaces.

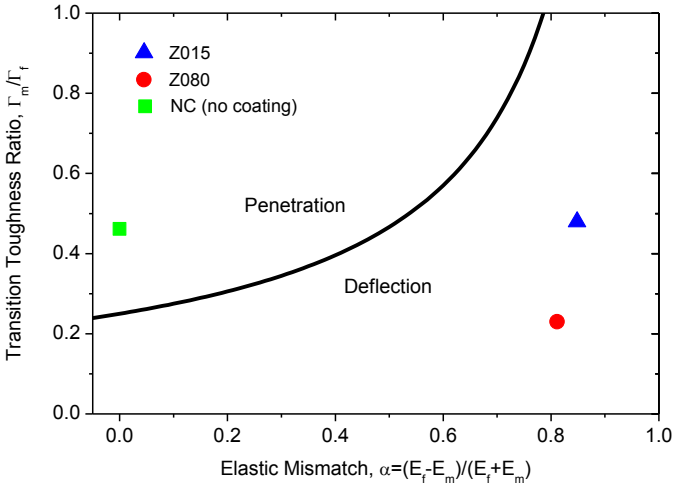

5.2.3. Interfacial sliding stress (fibre pushin test)

The interfacial sliding stress, τ, was determined via a modified fibre pushin test as described in Section 3.5.2 and 4.2.4. An example of the resulting curves of the second and third loops, are presented in Figure 32. Figure 33 presents a typical loop width curve with its respective fitting used for the sliding stress estimation.

The fibre pushin test yielded relatively high scattering of the values for both interface compositions (Figure 34). This problem has been also addressed by the author of the test.[46] The average interfacial sliding stress for the Z015 and Z080 interfaces was 123.8 ± 55.5 MPa and 120.4 ± 66.2 MPa, respectively and are statistically equal. .

The average sliding stress coincides with values found at the literature for zirconia interfaces,[10; 24; 27; 29] In this case, the contraction of the matrix around the interface and fibre during sintering can lead to high values due to the resulting compressive stresses. These stresses can play an important role on the sliding properties, thus overtaking the influence of the porosity and particle packing around the fibres. The sintering temperature produces significant roughness of the fibre surface (Figure 35) which could also explain high values of sliding stress.

Figure 32.Typical curve for the fibre pushin test showing the second and third loops.

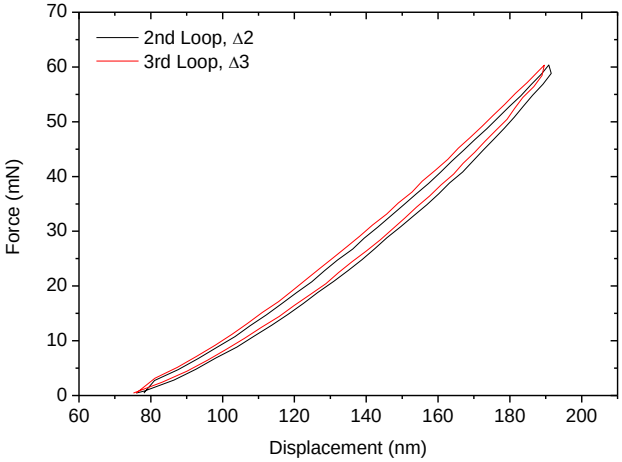

Figure 33.Diagram presenting a typical measured loop width and the respective fitting for estimation of the sliding stress.

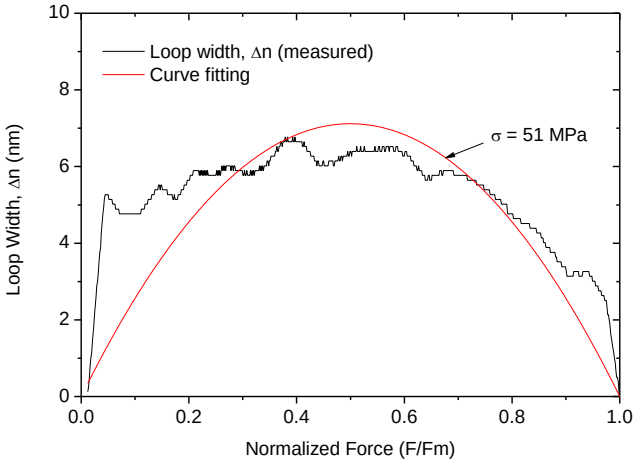

Figure 34.Cumulative distribution of the interfacial sliding stress results.

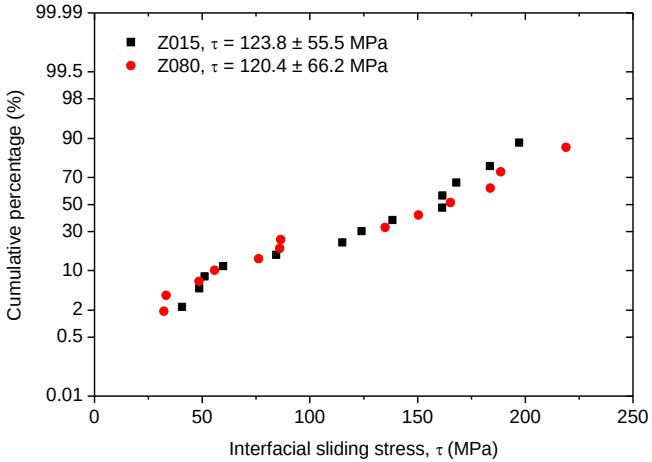

Figure 35.SEM image showing the fibre roughness after sintering at 1350 °C.

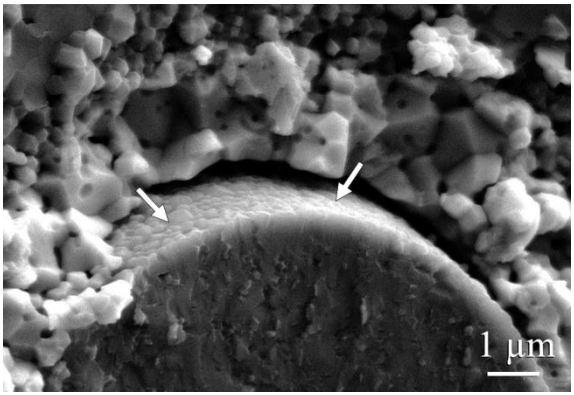

5.2.4. Fibre pullout

Other important toughening mechanism is the fibre pullout (Section 3.3). Model composites containing several coated fibres were tested. The fracture surface was then analysed in order to evaluate if the fibres were pulled out of the matrix during the fracture process.

Figure 36 shows SEM images of the fibre pullout for the Z015 composition. Although, its length is small, low interaction of the interface with the fibres can be seen. Figure 37 presents SEM images of the fibre pullout for the Z080 interface. In general, relatively short pullout lengths were encountered.

Some difficulties in characterising this phenomenon were encountered due to the small amount of fibres inside the model composite. Usually composites with fibre bundles present more evident fibre pullout, so, for adequate evaluation, a proper composite would be needed.

Figure 36.SEM image of the fibre pullout toughening mechanism of the Z015 interface.

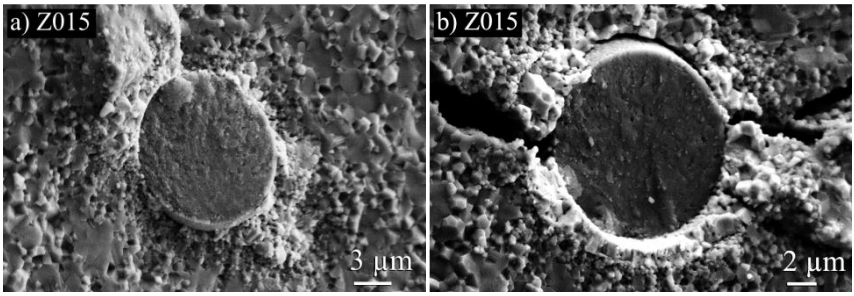

Figure 37.SEM image of the fibre pullout toughening mechanism of the Z080 interface.

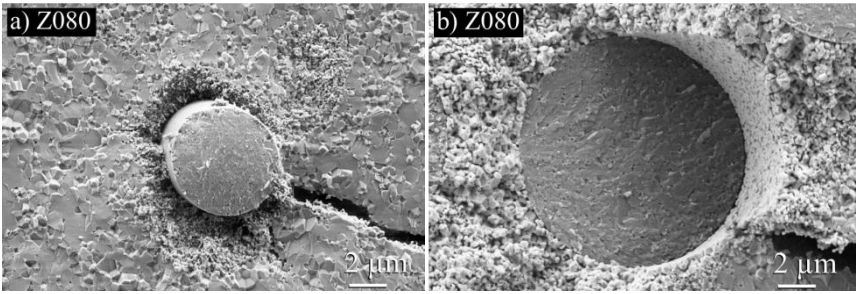

6. CONCLUSION

Toughening mechanism play an important role on the mechanical behaviour of ceramic matrix composites. For the toughening mechanics to be effective, the interface between fibre and matrix muss be tailored. Usually, a weak interface is needed. In addition, the interface must not react with the fibres, degrading their mechanical properties. It must also be stable at high temperatures and present sufficiently weak bonding to the fibre in order to promote toughening mechanisms. Thus, monoclinic zirconia attends to these basic requirements and can be applied in alumina-alumina composites.

In this work, the production and characterization of monoclinic zirconia-based fibre-matrix interfaces was performed. It was shown that monoclinic zirconia is suitable as interface for alumina-based composites.

The dip-coating process has shown to be an easy method of coating fibres and producing fibre-matrix interfaces. Uniform coating thicknesses were achieved using this method. Moreover, the coating porosity can be tailored varying the particle size of the dip-coating suspension.

Monoclinic zirconia presented low fracture toughness, therefore, low fracture energy produced in part by cracks present within the microstructure. The low fracture energy enables the interface to deflect cracks impinging the fibres, which is shown with the He and Hutchinson crack deflection diagram and proven by Vickers indentation tests.

The fibre pullout toughening mechanism was also presented, although not so evident due to the configuration of the model composite and the test.

The interfacial sliding stress was accessed, however, with high scattering of the results. In this test, no significant difference between the two interfaces was found.

Not significant difference between the two monoclinic zirconia coatings was presented. According to the work proposal, both particle sizes showed to be suitable for fibre-matrix interfaces in alumina-based CMCs.

Monoclinic zirconia has attended all requirements established in this work, showing to be suitable for development of fibre-matrix interfaces for alumina-alumina composites.

7. SUGGESTIONS FOR FUTURE WORK

- Produce long fibre composites to access their mechanical properties and compare among different coating porosities as well as with the absence of fibre coating.
- Test composites in four-point bending at high temperature (> 1170 °C) to evaluate the influence of the monoclinic to tetragonal phase transformation (decrease in 4% volume) and toughening mechanisms.
- Assess the residual stresses and influence of the roughness on the fibre-interface system.

8. REFERENCES

[1] CHAWLA, K. K. **Ceramic matrix composites**. London: Chapman & Hall, 1993. xii, 423 p

[2] KRENKEL, W. **Ceramic matrix composites : fiber reinforced ceramics and their applications**. Weinheim: Wiley-VCH, 2008. xxi, 418 p.

[3] BLAESE, D. **Mode II interlaminar fracture behaviour of Carbon-Carbon composites**. 2010. 81p (Diploma Thesis) Universität Bremen, Bremen.

[4] HABLITZEL, M. P.; GARCIA, D. E.; HOTZA, D. Interfaces fracas em compósitos de matriz cerâmica de alumina/alumina. **Matéria (Rio de Janeiro),** v. 16, p. 788-794, 2011.

[5] DAVIS, J. B.; LOFVANDER, J. P. A.; EVANS, A. G.; BISCHOFF, E.; EMILIANI, M. L. Fiber Coating Concepts for Brittle-Matrix Composites. **Journal of the American Ceramic Society,** v. 76, n. 5, p. 1249-1257, May 1993.

[6] BANSAL, N. P. **Handbook of ceramic composites**. Boston: Kluwer Academic Publishers, 2005. x, 554 p.

[7] MATTONI, M. A.; YANG, J. Y.; LEVI, C. G.; ZOK, F. W. Effects of matrix porosity on the mechanical properties of a porous-matrix, all-oxide ceramic composite. **Journal of the American Ceramic Society,** v. 84, n. 11, p. 2594-2602, Nov 2001.

[8] ZOK, F. W.; LEVI, C. G. Mechanical properties of porous-matrix ceramic composites. **Advanced Engineering Materials,** v. 3, n. 1-2, p. 15-23, Jan 2001.

[9] BERROTH, K. E.; HASLAM, J. J.; LANGE, F. F. Processing and properties of an all-oxide composite with a porous matrix. **Journal of the European Ceramic Society,** v. 20, n. 5, p. 607-618, 2000.

[10] KERANS, R. J.; HAY, R. S.; PARTHASARATHY, T. A.; CINIBULK, M. K. Interface design for oxidation-resistant ceramic composites. **Journal of the American Ceramic Society,** v. 85, n. 11, p. 2599-2632, Nov 2002.

[11] FABER, K. T. Ceramic composite interfaces: Properties and design. **Annual Review of Materials Science,** v. 27, p. 499-524, 1997.

[12] BRENNAN, J. J.; PREWO, K. M. Silicon-Carbide Fiber Reinforced Glass-Ceramic Matrix Composites Exhibiting High-Strength and Toughness. **Journal of Materials Science,** v. 17, n. 8, p. 2371-2383, 1982.

[13] LUH, E. Y.; EVANS, A. G. High-Temperature Mechanical-Properties of a Ceramic Matrix Composite. **Journal of the American Ceramic Society,** v. 70, n. 7, p. 466-469, Jul 1987.

[14] MORGAN, P. E. D.; MARSHALL, D. B. Ceramic Composites of Monazite and Alumina. **Journal of the American Ceramic Society,** v. 78, n. 6, p. 1553-1563, Jun 1995.

[15] MORGAN, P. E. D.; MARSHALL, D. B.; HOUSLEY, R. M. High-Temperature Stability of Monazite-Alumina Composites. **Materials Science and Engineering a-Structural Materials Properties Microstructure and Processing,** v. 195, n. 1-2, p. 215-222, Jun 1 1995.

[16] CINIBULK, M. K.; HAY, R. S. Textured magnetoplumbite fiber-matrix interphase derived from sol-gel fiber coatings. **Journal of the American Ceramic Society,** v. 79, n. 5, p. 1233-1246, May 1996.

[17] HE, M. Y.; HUTCHINSON, J. W. Crack Deflection at an Interface between Dissimilar Elastic-Materials. **International Journal of Solids and Structures,** v. 25, n. 9, p. 1053-1067, 1989.

[18] CARPENTER, H. W.; BOHLEN, J. W. **Method of forming a precracked fiber coating for toughening ceramic fiber-matrix**

composites. US Patent 5,110,771: Northrop Corporation**:** 6 p. 1992.

[19] RUF, H.; EVANS, A. G. Toughening by Monoclinic Zirconia. **Journal of the American Ceramic Society,** v. 66, n. 5, p. 328-332, 1983.

[20] RICHERSON, D. W. **Modern ceramic engineering : properties, processing, and use in design**. 2nd. New York: Marcel Dekker, 1992. xiii, 860 p.

[21] STEMPIN, J. L.; WEXELL, D. R. **Fiber reinforced ceramic matrix composites exhibiting improved high-temperature strength**. US Patent 5,422,319: Corning Incorporated**:** 10 p. 1995.

[22] COLOMBAN, P.; BRUNETON, E.; LAGRANGE, J. L.; MOUCHON, E. Sol-gel mullite matrix-SiC and -mullite 2D woven fabric composites with or without zirconia containing interphase: Elaboration and properties. **Journal of the European Ceramic Society,** v. 16, n. 2, p. 301-314, 1996.

[23] KRUGER, R.; BOCKMEYER, M. J. Influence of precursor densification on strength retention of zirconia-coated Nextel (TM) 610 fibers. **Journal of the American Ceramic Society,** v. 91, n. 4, p. 1070-1076, Apr 2008.

[24] UTKIN, A. V.; MATVIENKO, A. A.; TITOV, A. T.; BAKLANOVA, N. I. Multiple zirconia interphase for SiC/SiC(f) composites. **Surface & Coatings Technology,** v. 205, n. 8-9, p. 2724-2729, Jan 25 2011.

[25] LEE, W. Y.; LARA-CURZIO, E.; MORE, K. L. Multilayered oxide interphase concept for ceramic-matrix composites. **Journal of the American Ceramic Society,** v. 81, n. 3, p. 717-720, Mar 1998.

[26] LI, H.; LEE, J.; LIBERA, M. R.; LEE, W. Y.; KEBBEDE, A.; LANCE, M. J.; WANG, H. Y.; MORSCHER, G. N. Morphological evolution and weak interface development within

chemical-vapor-deposited zirconia coating deposited on Hi-Nicalon (TM) fiber. **Journal of the American Ceramic Society,** v. 85, n. 6, p. 1561-1568, Jun 2002.

[27] LI, H.; MORSCHER, G. N.; LEE, J.; LEE, W. Y. Tensile and stress-rupture behavior of SiC/SiC minicomposite containing chemically vapor deposited zirconia interphase. **Journal of the American Ceramic Society,** v. 87, n. 9, p. 1726-1733, Sep 2004.

[28] GU, X.; TRUSTY, P. A.; BUTLER, E. G.; PONTON, C. B. Deposition of zirconia sols on woven fibre preforms using a dip-coating technique. **Journal of the European Ceramic Society,** v. 20, n. 6, p. 675-684, May 2000.

[29] PARTHASARATHY, T. A.; BOAKYE, E. E.; KELLER, K. A.; HAY, R. S. Evaluation of porous ZrO2-SiO2 and monazite coatings using Nextel (TM) 720-fiber-reinforced Blackglas (TM) minicomposites. **Journal of the American Ceramic Society,** v. 84, n. 7, p. 1526-1532, Jul 2001.

[30] BOAKYE, E. E.; HAY, R. S.; PETRY, M. D.; PARTHASARATHY, T. A. Zirconia-silica-carbon coatings on ceramic fibers. **Journal of the American Ceramic Society,** v. 87, n. 10, p. 1967-1976, Oct 2004.

[31] HILLIG, W. B. Strength and Toughness of Ceramic Matrix Composites. **Annual Review of Materials Science,** v. 17, p. 341-383, 1987.

[32] BAO, G.; SUO, Z. Remarks on Crack-Bridging Concepts. **Applied Mechanics Reviews,** v. 45, n. 8, p. 355-366, 1992.

[33] ERGUN, H.; BODUROGLU, H. Fiber volume ratio effect on the crack bridging mechanism in uniaxial reinforced ceramic composites. **Materials Science and Engineering a-Structural Materials Properties Microstructure and Processing,** v. 387, p. 882-886, Dec 15 2004.

[34] HUTCHINSON, J. W.; JENSEN, H. M. Models of Fiber Debonding and Pullout in Brittle Composites with Friction (Vol 9, Pg 139, 1990). **Mechanics of Materials,** v. 14, n. 3, p. 221-221, Jan 1993.

[35] EVANS, A. G.; ZOK, F. W. The Physics and Mechanics of Fiber-Reinforced Brittle-Matrix Composites. **Journal of Materials Science,** v. 29, n. 15, p. 3857-3896, Aug 1 1994.

[36] GOUSHEGIR, S. M.; GUGLIELMI, P. O.; DA SILVA, J. G. P.; HABLITZEL, M. P.; HOTZA, D.; AL-QURESHI, H. A.; JANSSEN, R. Fiber-Matrix Compatibility in an All-Oxide Ceramic Composite with RBAO Matrix. **Journal of the American Ceramic Society,** v. 95, n. 1, p. 159-164, Jan 2012.

[37] BRINKER, C. J.; SCHERER, G. W. **Sol-gel science : the physics and chemistry of sol-gel processing**. Boston: Academic Press, 1990. xiv, 908 p.

[38] PHARR, G. M. Measurement of mechanical properties by ultra-low load indentation. **Materials Science and Engineering a-Structural Materials Properties Microstructure and Processing,** v. 253, n. 1-2, p. 151-159, Sep 30 1998.

[39] PHARR, G. M.; OLIVER, W. C.; BROTZEN, F. R. On the Generality of the Relationship among Contact Stiffness, Contact Area, and Elastic-Modulus during Indentation. **Journal of Materials Research,** v. 7, n. 3, p. 613-617, Mar 1992.

[40] HAY, J. Introduction to Instrumented Indentation Testing. **Experimental Techniques,** v. 33, n. 6, p. 66-72, Nov-Dec 2009.

[41] BRAM, M.; NELLES, H.; BUCHKREMER, H. P.; STOVER, D. Characterization, mechanical properties and deformation behavior of highly porous materials made of titanium and stainless steel (316L). **Materialwissenschaft Und Werkstofftechnik,** v. 31, n. 6, p. 497-500, Jun 2000.

42 3M Ceramic Fibre Products, Nextel(TM) Ceramic Fibre Technical Notebook, St. Paul, MN, USA.

43 LY Laboratory Facilities, Available in: http://web.hku.hk/~ylin/facilities.html, Acessed in: february 13th, 2013.

44 OLIVER, W. C.; PHARR, G. M. An Improved Technique for Determining Hardness and Elastic-Modulus Using Load and Displacement Sensing Indentation Experiments. **Journal of Materials Research,** v. 7, n. 6, p. 1564-1583, Jun 1992.

45 MARSHALL, D. B.; OLIVER, W. C. Measurement of Interfacial Mechanical-Properties in Fiber-Reinforced Ceramic Composites. **Journal of the American Ceramic Society,** v. 70, n. 8, p. 542-548, Aug 1987.

46 WEAVER, J. H.; RANNOU, J.; MATTONI, M. A.; ZOK, F. W. Interface properties in a porous-matrix oxide composite. **Journal of the American Ceramic Society,** v. 89, n. 9, p. 2869-2873, Sep 2006.

47 ZOK, F. W. Developments in oxide fiber composites. **Journal of the American Ceramic Society,** v. 89, n. 11, p. 3309-3324, Nov 2006.

48 KUBLER, J. J. Fracture toughness of ceramics using the SEVNB method: From a preliminary study to a standard test method. **Fracture Resistance Testing of Monolithic and Composite Brittle Materials,** v. 1409, p. 93-106, 2002.

49 CONSULTANTS BUREAU. **Powder metallurgy and metal ceramics**. New York: Consultants Bureau**:** v. p. 1993.

50 RAJENDRAN, N.; DEVI, K. B.; SINGH, K. Sol-gel synthesis and characterisation of nanoporous zirconium titanate coated on 316L SS for biomedical applications. **Journal of Sol-Gel Science and Technology,** v. 59, n. 3, p. 513-520, Sep 2011.

[51] KHOMAMI, B.; ABEDIJABERI, A.; BHATARA, G.; SHAQFEH, E. S. G. A computational study of the influence of viscoelasticity on the interfacial dynamics of dip coating flow. **Journal of Non-Newtonian Fluid Mechanics,** v. 166, n. 12-13, p. 614-627, Jul 2011.

[52] YE, H.; XU, J.; YIN, Y.; MA, H. M.; LIU, X. A novel trilayer antireflection coating using dip-coating technique. **Chinese Optics Letters,** v. 9, n. 7, Jul 10 2011.

[53] ECHEBERRIA, J.; TARAZONA, J.; HE, J. Y.; BUTLER, T.; CASTRO, F. Sinter-HIP of alpha-alumina powders with sub-micron grain sizes. **Journal of the European Ceramic Society,** v. 22, n. 11, p. 1801-1809, Oct 2002.

[54] CHAISITSAK, S. Nanocrystalline SnO(2):F Thin Films for Liquid Petroleum Gas Sensors. **Sensors,** v. 11, n. 7, p. 7127-7140, Jul 2011.

[55] TEHRANI, F. M. K.; RASHIDZADEH, M.; NEMATI, A.; IRANDOUKHT, A.; FARIDNIA, B. Characterization and photocatalytic activities of nanosized titanium dioxide thin films. **International Journal of Environmental Science and Technology,** v. 8, n. 3, p. 545-552, Sum 2011.

[56] YAHIA, I. S.; OSIRIS, W. G.; FARAG, A. A. M. Extraction of the device parameters of Al/P(3)OT/ITO organic Schottky diode using J-V and C-V characteristics. **Synthetic Metals,** v. 161, n. 11-12, p. 1079-1087, Jun 2011.

[57] MUNOZ-TABARES, J. A.; JIMENEZ-PIQUE, E.; REYES-GASGA, J.; ANGLADA, M. Microstructural changes in ground 3Y-TZP and their effect on mechanical properties. **Acta Materialia,** v. 59, n. 17, p. 6670-6683, Oct 2011.

[58] KÜBLER, J. Fracture Toughness of Ceramics Using the Sevnb Method: Preliminary Results. In: (Ed.). **Proceedings of the 21st Annual Conference on Composites, Advanced Ceramics, Materials, and Structures—B: Ceramic Engineering and**

Science Proceedings: John Wiley & Sons, Inc., 2008. p.155-162. ISBN 9780470294444.

[59] JELITTO, H.; FELTEN, F.; SWAIN, M. V.; BALKE, H.; SCHNEIDER, G. A. Measurement of the total energy release rate for cracks in PZT under combined mechanical and electrical loading. **Journal of Applied Mechanics-Transactions of the Asme,** v. 74, n. 6, p. 1197-1211, Nov 2007.

[60] BOUDOUKHA, L.; HALITIM, F.; PALETTO, S.; FANTOZZI, G. Mechanical properties of titanium implanted polycrystalline alumina and sapphire determined by nanoindentation. **Ceramics International,** v. 24, n. 3, p. 189-198, 1998.

[61] MUNRO, R. G. Evaluated material properties for a sintered alpha-alumina. **Journal of the American Ceramic Society,** v. 80, n. 8, p. 1919-1928, Aug 1997.

[62] XU, Z. R.; CHAWLA, K. K.; LI, X. Effect of High-Temperature Exposure on the Tensile-Strength of Alumina Fiber Nextel 610. **Materials Science and Engineering a-Structural Materials Properties Microstructure and Processing,** v. 171, n. 1-2, p. 249-256, Nov 1 1993.

[63] GOUSHEGIR, S. M.; GUGLIELMI, P. O.; OLIVEIRA, A. P. N.; HOTZA, D.; JANSSEN, R. Fiber-Matrix Compatibility in LZSA Glass-Ceramic Matrix Composites. **Advanced Powder Technology Viii, Pts 1 and 2,** v. 727-728, p. 562-567, 2012.

[64] SCHMUCKER, M.; MECHNICH, P. Improving the Microstructural Stability of Nextel (TM) 610 Alumina Fibers Embedded in a Porous Alumina Matrix. **Journal of the American Ceramic Society,** v. 93, n. 7, p. 1888-1890, Jul 2010.